Determination of an Optimum Sector Size for Plan Position Indicator Measurements using a Long Range Coherent Scanning Atmospheric Doppler LiDAR.

Simon, Elliot

Publication date:
2015

Document Version
Publisher's PDF, also known as Version of record

UPPSALA UNIVERSITET

DTU

Determination of an Optimum Sector Size for Plan Position Indicator Measurements using a Long Range Coherent Scanning Atmospheric Doppler LiDAR

Elliot I. Simon
elliot@elliot-simon.com

Uppsala University
Department of Earth Sciences

September 2015

Author: Elliot I. Simon
Title: Determination of an Optimum Sector Size for Plan Position Indicator Measurements using a Long Range Coherent Scanning Atmospheric Doppler LiDAR

Department: Department of Earth Sciences
University: Uppsala University

Project Summary / Abstract:

As wind energy plants continue to grow in size and complexity, advanced measurement technologies such as scanning Doppler LiDAR are essential for assessing site conditions and prospecting new development areas.

The RUNE project was initiated to determine best practices for the use of scanning LiDARs in resource assessments for near shore wind farms. The purpose of this thesis is to determine the optimum configuration for the plan position indicator (PPI) scan type of a scanning LiDAR. A task specific Automated Analysis Software (AAS) is created, and the sensitivity of the integrated velocity azimuth process (iVAP) reconstruction algorithm is examined using sector sizes ranging from 4 to 60 degrees. Further, a comparison to simultaneous dual Doppler measurement is presented in order to determine the necessity of deploying two LiDARs rather than one.

DTU has developed a coordinated long range coherent scanning multi-LiDAR array (the WindScanner system) based on modified Leosphere WindCube 200S devices and an application specific software framework and communication protocol. The long range WindScanner system was deployed at DTU's test station in Høvsøre, Denmark and measurement data was collected over a period of 7 days. One WindScanner was performing 60 degree sector scans, while two others were placed in staring dual Doppler mode. All three beams were configured to converge atop a 116.5m instrumented meteorological mast.

A significant result was discovered which indicates that the accuracy of the reconstructed measurements do not differ significantly between sector sizes of 30 and 60 degrees. Using the smallest sector size which does not introduce systematic error has numerous benefits including: increasing the scan speed, measurement distance and angular resolution.

When comparing collocated dual Doppler, sector scan and in-situ met-mast instrumentation, we find very good agreement between all techniques. Dual Doppler is able to measure wind speeds within 0.1%, and 60 degree sector scan within 0.2% on average of the reference values. For retrieval of wind direction, the sector scan approach performs particularly well. This is likely attributable to lower errors introduced by the assumption of flow field homogeneity over the scanned area, in contract to wind direction which tends to be more non-uniform. For applications such as site resource assessments, where generally accurate 10 minute wind speed and direction values are required, a scanning LiDAR performing PPI scans with a sector size of between 30 and 38 degrees is recommended. The laser's line of sight path should be directed parallel to the predominant wind direction and at the lowest elevation angle possible.

MSc Thesis Report
September, 2015

Project period:
2015.03.15 - 2015.09.22

ECTS:
[15]

Education:
Master of Science [M.Sc.]

Field:
Renewable Energy Technology
Wind Power Project Management

Supervisors:
Professor Jens Nørkær Sørensen
(DTU & Uppsala University)
Dr. Nikola Vasiljević
(DTU-Risø, Post-Doctoral Researcher)
Guillaume Léa, MSc
(DTU-Risø, Senior Development Engineer)

Remarks:
This report is submitted as partial fulfillment of the requirements for graduation in the above education at Uppsala University, Sweden.

Sponsorship:
Erasmus+ Traineeship Grant
Swedish-American Chamber of Commerce in NYC Graduate Fellowship

Pages: 76
Tables: 11
Figures: 51
References: 31

DETERMINATION OF AN OPTIMUM SECTOR SIZE FOR PLAN POSITION INDICATOR

MEASUREMENTS USING A LONG RANGE COHERENT SCANNING ATMOSPHERIC DOPPLER LIDAR

Dissertation in partial fulfilment of the requirements for the degree of:

MASTER OF SCIENCE WITH A MAJOR IN RENEWABLE ENERGY TECHNOLOGY WITH A FOCUS ON WIND POWER PROJECT MANAGEMENT

UPPSALA
UNIVERSITET

Uppsala University
Department of Earth Sciences

Supervisors:

Professor Jens Nørkær Sørensen

Dr. Nikola Vasiljević

Guillaume Léa, MSc

Examiner: Professor Simon-Philippe Breton

22 September 2015

Preface & Acknowledgements

This project was completed in residence at DTU Wind Energy (Risø) in Roskilde, Denmark within the Test and Measurement section (TEM). TEM focuses on developing instrumentation which can accurately measure characteristics of the atmosphere and then applies experimental methodologies to verify and improve measurement techniques and applied climate models used within the global wind energy industry.

My biggest gratitude in completing this thesis work goes to all my colleagues at DTU Wind Energy, and TEM in particular. I have discovered the secret to productive and rewarding work- the environment and people you interact with. Everyone has been so kind and helpful to me in every way since I first arrived in Denmark. It has definitely not gone unappreciated!

Undoubtedly the biggest contributors to this project and my growing competency in engineering and wind energy research are my mentors and friends, Guillaume Léa and Nikola Vasiljević. It has been a real pleasure to work with and learn from you both.

It is also with great appreciation that I thank and acknowledge key financial support from the European Union's Erasmus+ Traineeship Grant as well as the Swedish-American Chamber of Commerce in NYC's Graduate Fellowship. Both have played a vital part in helping to develop my academic and professional goals, and I pledge to pay the generosity forward so that others may gain from the same opportunities that I have been afforded.

I would also like to credit the European Wind Energy Agency (EWEA) for providing the platform (Offshore 2015 Conference in København) to meet industry and academic leaders and discuss my ideas within such a supportive atmosphere. Further, I would also like to recognise my friends and colleagues in Uppsala and Visby and thank Professors Jens N. Sørensen and Heracles Polatidis for their overwhelming encouragement to undertake this project and for the great deal of respect they showed me during our time together.

Lastly, I would like to devote this endeavour to my family. Who have always encouraged and supported me in the most compelling ways. Much love to you all.

Elliot I. Simon
Roskilde, Denmark
September, 2015

Terminology

β	y intercept at x=0
θ	Azimuth angle (in degrees)
λ	Wavelength
φ	Elevation/altitude angle (in degrees)
3/4G	3rd/4th Generation Mobile Data Network (2 Mbit/s+)
3D	3 Dimensions/al
AAS	Automated Analysis Software
AOM	Acoustic Optic Modulator
CNR	Carrier to Noise Ratio
CW	Continuous Wave (laser)
DD	Dual Doppler
dir	Wind Direction (degrees)
DTU	Technical University of Denmark (*Danmarks Tekniske Universitet*)
EDFA	Erbium Doped Fibre (Optical) Amplifier
FFT	Fast Furrier Transform
FPGA	Field Programmable Gate Array
GPS	Global Positioning System
InGaAs	Indium gallium arsenide
LAN	Local Area Network
LiDAR	Light Detection and Ranging
LOS	Line of Sight
Met-Mast	Meteorological mast
MLE	Maximum Likelihood Estimator
NaN	Not a Number, Undefined, Unrepresented
PPI	Plan Position Indicator
PRF	Pulse Repetition Frequency
RHI	Range Height Indicator
RUNE	Reducing the Uncertainty of Near-shore Energy
SFTP	Secure File Transfer Protocol (encrypted)
SSvsDD	Sector Scan vs. Dual Doppler Campaign (Høvsøre, DK)
UU	Uppsala University (*Uppsala Universitet*)
VAD	Velocity Azimuth Display
VAP	Velocity Azimuth Process
ws	Wind Speed (m/s)

Contents

Figures

Tables

1 Project Summary / Abstract

As wind energy plants continue to grow in size and complexity, advanced measurement technologies such as scanning Doppler LiDAR are essential for assessing site conditions and prospecting new development areas.

The RUNE project was initiated to determine best practices for the use of scanning LiDARs in resource assessments for near shore wind farms. The purpose of this thesis is to determine the optimum configuration for the plan position indicator (PPI) scan type of a scanning LiDAR. A task specific Automated Analysis Software (AAS) is created, and the sensitivity of the integrated velocity azimuth process (iVAP) reconstruction algorithm is examined using sector sizes ranging from 4 to 60 degrees. Further, a comparison to simultaneous dual Doppler measurement is presented in order to determine the necessity of deploying two LiDARs rather than one.

DTU has developed a coordinated long range coherent scanning multi-LiDAR array (the WindScanner system) based on modified Leosphere WindCube 200S devices and an application specific software framework and communication protocol. The long range WindScanner system was deployed at DTU's test station in Høvsøre, Denmark and measurement data was collected over a period of 7 days. One WindScanner was performing 60 degree sector scans, while two others were placed in staring dual Doppler mode. All three beams were configured to converge atop a 116.5m instrumented meteorological mast.

A significant result was discovered which indicates that the accuracy of the reconstructed measurements do not differ significantly between sector sizes of 30 and 60 degrees. Using the smallest sector size which does not introduce systematic error has numerous benefits including: increasing the scan speed, measurement distance and angular resolution.

When comparing collocated dual Doppler, sector scan and in-situ met-mast instrumentation, we find very good agreement between all techniques. Dual Doppler is able to measure wind speeds within 0.1%, and 60 degree sector scan within 0.2% on average of the reference values. For retrieval of wind direction, the sector scan approach performs particularly well. This is likely attributable to lower errors introduced by the assumption of flow field homogeneity over the scanned area, in contract to wind direction which tends to be more non-uniform. For applications such as site resource assessments, where generally accurate 10 minute wind speed and direction values are required, a scanning LiDAR performing PPI scans with a sector size of between 30 and 38 degrees is recommended. The laser's line of sight path should be directed parallel to the predominant wind direction and at the lowest elevation angle possible.

2 Background & Introduction

2.1 Motivation of Study

With the increasing global expansion of large wind power projects, site developers, banks, utility companies, etc. require highly reliable and accurate measurements with which to predict electricity production (i.e. revenue) and model risk. Further, researchers within the wind energy field demand new tools and methods with which to investigate atmospheric phenomena, such as wake propagation, meteorological events, complex flow, etc. Conventional techniques such as the met-mast and in-situ anemometer provide only a single point measurement which is insufficient for the needs of modern users.

The Test and Measurement (TEM) section of DTU Wind Energy has developed a coherent Doppler scanning lidar known as the long-range WindScanner in partnership with Leosphere in France. The WindScanner system forms a time and space synchronised multi-LiDAR array which is capable of sampling radial wind speeds over a volume (3 dimensions). Currently the system is used as a research tool, with the ultimate goal of becoming a familiar and standardised instrument within the wind energy industry. For this to happen, accepted guidelines and procedures must be developed, documented and disseminated.

DTU, DONG Energy (currently the world's largest offshore wind developer) and DHI (the Danish Hydraulic Institute) have teamed up in the RUNE project to further understand atmospheric interactions in coastal zones. This study will be used to improve mesoscale wind atlases (for example the NEWA- New European Wind Atlas project) as well as assist in resource assessment and planning for near shore (defined here as <10km from land) wind farms. One of the main research questions to be answered within the RUNE project is to determine exactly how many LiDARs are necessary to accurately perform a resource assessment and in what configuration should they be placed.

The RUNE project and countless other applications of the WindScanner systems will employ a plan position indicator (PPI), or sector scanning strategy. Theoretical predictions on the optimal configuration of a PPI scan have been made, however comparisons to actual in-field measurements are needed in order to obtain the highest quality data during the experiments. This thesis is focused on providing insight into optimal PPI scanning trajectories and configurations which will then be used within RUNE and subsequent measurement campaigns.

2.2 Thesis Objective: Optimum Sector Size

The objective of this thesis is to determine the optimum sector size to be used when designing measurement scenarios employing the plan position indicator (PPI) scan type. Scanning LiDARs have a somewhat fixed measurement duration (mainly due to the scanner head movement and acquisition of the reflected laser pulse). Therefore, a trade-off exists between measuring over a larger area and the rate of sampling. If it is determined that smaller sector sizes perform as well (or better) than larger ones when compared to the accepted reference instrument (cup anemometer), then some of the following improvements could be realised:

- ⊕ Faster refresh rates over the area sampled, since the angular size is smaller
- ⊕ Improved resolution by incorporating more line of sight measurements within the sector area

- ⊕ Increased measurement distance, since more time could be spent on lengthening the reflected pulse acquisition time
- ⊕ Better averaging (e.g. 10 minute) results due to the larger number of samples included in the average
- ⊕ Better representation of the targeted region, especially at far distances where a large sector size could envelop a vast area

To explore this research question, coherent scanning LiDAR technology will be presented, along with the theoretical background of PPI reconstructions and an experimental campaign which will demonstrate the accuracy of various sector sizes against a reference cup anemometer as well as dual Doppler LiDAR.

2.3 LiDAR

2.3.1 Principles and Operation

LiDAR (Light Detection and Ranging) is an innovative remote sensing technology with untold uses across all fields of science and engineering (e.g. meteorological measurements, mapping, military and even malaria prevention). For atmospheric modelling and wind power development, we are particularly interested in retrieving wind speed and direction measurements over an area or volume. This data has unbounded applications, especially when compared with traditional anemometry approaches. For a researcher- in helping to better understand fluid dynamics and improve flow and turbulence models. To an engineer or project developer- in order to optimise turbine designs and power plant layouts for specific site conditions, or even to provide automated turbine and farm level control.

In the case of atmospheric sampling, a LiDAR begins operation by emitting a laser beam (continuous wave or pulse) into the atmosphere. Laser light is characterised by spatial coherence, which means that the beam is focused to a narrow width over great distances, and does not diffuse quickly as with most other light sources. This spatial coherence is due to the collimation of the emitted light (with rays running in parallel) created either by a collimating telescope, or by parallel mirrors in the laser's optical cavity (Premasundaran, 2015). Therefore, the beam expands only negligibly over large distances, allowing for high resolution sampling even at the tens of kilometres range. Further, laser emitters are also capable of high temporal coherence, where the emitted beam exists in a very narrow spectral width over the entire path of travel. (Paschotta, 2015)

Once the laser beam is transmitted, it interacts with micron sized aerosols (dust, water vapour/droplets, smoke, pollutants, etc.) in the atmosphere primarily through Mie scattering (Mie, 1908). It is assumed that these particles are travelling at the same speed as the wind. A very small portion of the laser beams will backscatter against the aerosols (reflect 180 degrees) and land back on the photodetector of the LiDAR device.

A physical phenomenon known as the Doppler Effect is used to retrieve the radial wind speed from the captured backscattered light. When the laser beam interacts with an atmospheric aerosol, its wavelength is shifted respective to the line of sight

(LOS) speed of the aerosol. This radial velocity is a projection of the true wind speed along the laser's line of sight. For aerosols moving towards the laser emitter, the frequency will increase; for aerosols moving away, the frequency will decrease. This allows for determining the sign of the radial velocity value. The general formula is given:

$$f = f_0 \, (1 + \frac{v}{c})$$

Where f = the observed frequency, f_0 = the emitted frequency, v = the velocity towards the source (radial velocity), and c = the speed of light (constant).

Since the frequency at emission is constant and known, it is simple to calculate the LOS wind speed from the captured backscatter by using the relationship:

$$\Delta f = \left(\frac{-2 \, v}{\lambda}\right)$$

Where Δf = Doppler (frequency) shift, v = the radial velocity, and λ = wavelength of the emitted light (source).

On-board signal processing software includes time gating of the backscattered pulses to allow multiple range gates (distances) to be measured simultaneously along a single LOS, up until the device's maximum range resolution (Vasiljević, 2014).

Pulsed LiDAR devices have a maximum theoretical range resolution of:

$$dist_{max}(km) = \frac{c}{PRF}$$

Where c = the speed of light (constant), and PRF represents the LiDAR's pulse repetition frequency (i.e. number of pulses per second). Therefore a LiDAR configured to use a 10 kHz PRF will have a theoretical maximum measurement range of 30km. In practice however, shorter acquisition times and imperfect atmospheric conditions will act to reduce the device's maximum range.

2.3.2 Coherent LiDAR

In contrast to simple direct detection LiDAR, which requires high energy laser sources and directly measures the amplitude of the backscatter signal, technology from the radio and telecommunications industry has been applied to develop a coherent, or indirect detection method. Coherent detection (particularly micropulse) LiDARs operate at lower power, allowing them to be comparatively eye safe and resolve frequency shifts with much higher sensitivity (Paschotta, 2015). In order to do this however, the transceiver systems gain considerable complexity.

Coherent LiDAR systems rely on the principle of optical heterodyne detection. In this, two frequencies (the source and a local oscillator) are modulated together to form two new signals at their sum and difference of their frequencies (Henderson, 2013). The basis for this can be demonstrated with the simplified identity:

$$\sin f_1 \sin f_2 = \frac{1}{2}\cos(f_1 - f_2) - \frac{1}{2}\cos(f_1 + f_2)$$

Where the left hand represents two sine wave signals which are mixed (multiplied), and the right hand is their resulting sum and difference heterodynes. The sum heterodyne is removed by a high pass filter to obtain the desired difference heterodyne, which represents the interference between the two signals (commonly known as a beat signal). This beat signal contains the same properties as the original signal (amplitude, phase, modulation), but oscillates at a much lower frequency which can be processed easily in high resolution by the photodetector.

2.3.3 Scanning LiDAR

The basic coherent LiDAR device outlined above does not include a movable targeting system, so measurements could only be collected for range gates (distances) along a single line of sight. The inclusion of a dual axis positioning system (scanner head) allows the laser beam to be directed at any unobstructed point in space (full dome) by jogging across motors controlling the azimuth and elevation angles.

Figure 1: WindCube 200S dual-axis scanner head

Through precise control of the dual-axis scanner head, it is possible to perform scans across an area or within a volume. Scanning patterns can be either simple or complex, as seen in Figure 2, and are carefully chosen to fit the intended application. The observed radial wind speeds will then be retrieved over the area or volume of the scan, usually repeating for a set length of time or indefinitely.

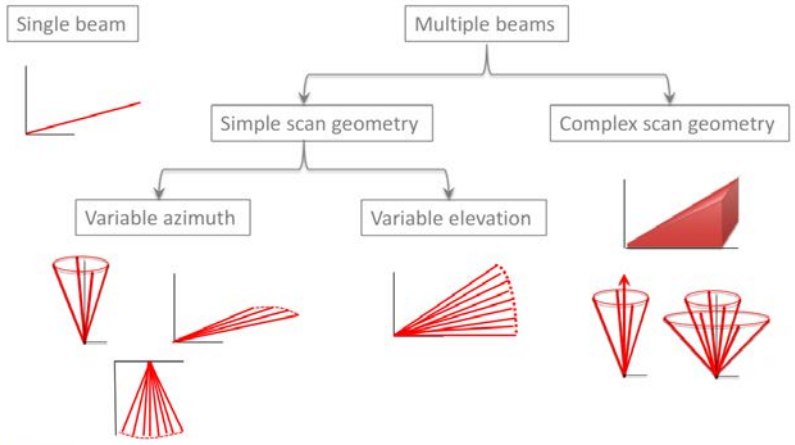

Figure 2: Examples of single LiDAR scan geometries
Source: SgurrEnergy Webinar (SgurrEnergy and Clive, 2014)

2.3.4 Plan Position Indicator

In the Plan Position Indicator (PPI) scan, the LiDAR scanner head is fixed to a constant elevation/altitude angle, and sweeps across an azimuth range with a constant speed. This allows for radial speed data to be collected across a conical section. For angles less than 360 degrees, this scan pattern is referred to as a "Sector Scan" (otherwise it is a "Surveillance Scan"). In a sector scan, usually the scanner head will reverse direction and scan forwards/backwards through the given azimuth range. It is also possible to reset to the starting azimuth value at the end of each scan and repeat.

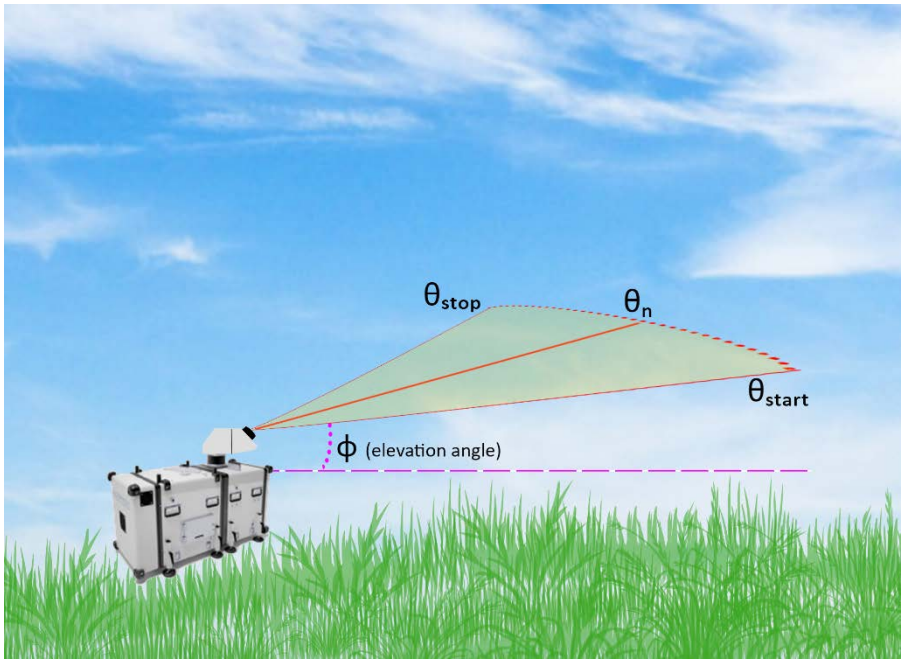

Figure 3: Sector scan (PPI) configuration

The figure above represents a typical sector scan setup. The sector size represents the angular area between the start and stop azimuth values. The elevation angle should be kept as low as possible in order to neglect the vertical component of the wind vector. More on the importance of a low elevation angle is presented in section: 4.3.2.

The common methods of reconstructing sector scan data involve point process least-squares fitting of the observed radial wind velocities to a sinusoidal curve in order to obtain wind speed and direction values for selected range gates across the scanned volume. More about retrieval algorithms and their respective equations is presented in section: 4.3.3.

2.3.5 Dual Doppler Mode

In dual Doppler mode, two LiDARs are placed such that their beams are crossed at a single point in space. In the simplest scenario, they operate in "staring mode" where the azimuth and elevation/altitude angles remain static (fixed) throughout the measurement period. With the long range WindScanner system, it is also possible to synchronise and direct the two beams along a complex trajectory (such as a virtual line, circle, Lissajous or rose pattern, etc.) depending on the intended application.

Independent LOS measurements from the two LiDARs can then be combined in order to obtain wind speed and direction information at the targeted point. This technique is presented and discussed in further detail within section: 4.3.4.

In order to obtain trustworthy measurements from a dual Doppler measurement scenario, it is extremely important to have a high degree of pointing accuracy within the scanner head as well as optical alignment of the telescope. Otherwise, the beams will not converge and portions of different wind vectors will be used together in the reconstruction. Therefore, it is standard practice to perform a hard target calibration of the scanner head (positioning system) upon deployment. The process for this in the Høvsøre campaign is documented below in section: 5.5.1.

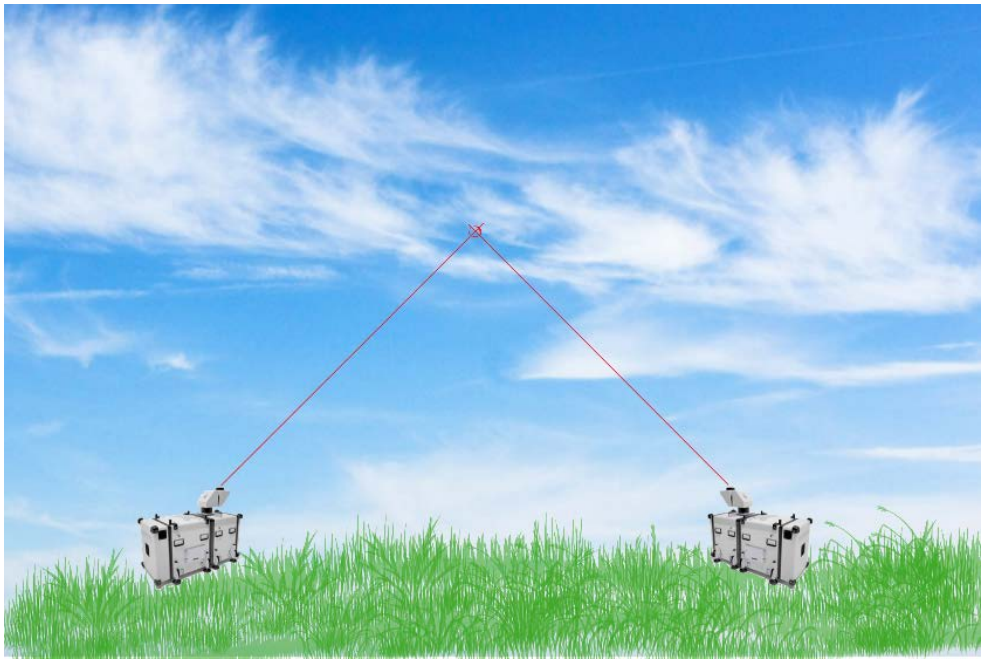

Figure 4: Dual-Doppler scanning configuration

2.4 WindScanner Platform

2.4.1 Introduction

The long range WindScanner platform is a networked remote sensing measurement system which is capable of controlling and monitoring numerous spatially separated LiDARs. The result of which is the ability to coordinate and carry out complex measurement scenarios previously considered onerous or unfeasible while also overseeing and directing operations remotely.

The combined DTU long range WindScanner measurement system currently consists of four modified Leosphere WindCube 200S units (WindScanners) as well as the DTU developed WindScanner software. The open platform is designed such that any LiDAR could be integrated into the system with minimal modifications, with the ultimate goal of becoming a standardised platform for both LiDAR field operations and data analysis.

2.4.2 Leosphere/DTU WindCube 200S

The long range WindScanner LiDAR was developed in cooperation with DTU Wind Energy (DK), Leosphere (F), Heason (UK) and IPU (DK). The hardware is sold commercially by Leosphere under the model name WindCube 200S, with a few hardware modification and completely separate software architecture that distinguishes the WindScanner branded systems. This is explained further in the following sections.

The WindCube 200S is a high powered, pulsed, coherent detection LiDAR equipped with a dual axis scanner head. The measurement process begins with a trigger signal, sent when the scanner head is pointing in the desired position. A customised FPGA circuit board generates a digital message signal (rectangular trigger), along with an analogue (Gaussian shaped) signal which is fed into the AOM (acousto-optic modulator). There, the two signals are modulated along with a local oscillator (CW laser at a wavelength of 1543nm). The AOM generates laser pulses with the correct shape and timing created from the continuous wave light source.

Next, the pulse is amplified within the EDFA to a mean power of 1W (Cariou et al., 2006). The amplified pulse exits a 100mm aperture collimating telescope and travels through the optical (mirrored) pathway (i.e. scanner head) until it is emitted through the external lens.

The emitted laser pulse interacts with airborne particles within the sampled area or volume. Some of the pulses will backscatter and arrive back at the telescope. An optical circulator transfers the received pulses through the same mirror path to a mixer, which again modulates the CW laser into backscattered signal. This outputs both the sum ($f_{AOM} + f_{CW} \pm \Delta f$) and difference ($f_{AOM} - f_{CW} \pm \Delta f$) heterodynes. The sum heterodyne is subsequently filtered out through the mixer's high pass filter. The remaining difference heterodyne frequency mixing results in the "beat phenomenon". The resulting signal comprises an amplitude which oscillates at the frequency difference between the input signals. The beat signal is then received in analogue

form by the InGaAs photodetector, which is then sampled and digitised by the acquisition board at 250 MHz (4 ns sampling frequency). (Cariou et al., 2006)

Once the (oscillating) backscatter signal is obtained, a fast Fourier transform (FFT) is applied. This converts the signal to the normalised frequency domain, which can then be analysed using statistical methods. The maximum likelihood estimation (MLE) technique is employed to estimate parameters of the transformed distribution, which then gives the desired radial speed value.

A graphical layout of the internal WindScanner hardware is depicted in the following figure:

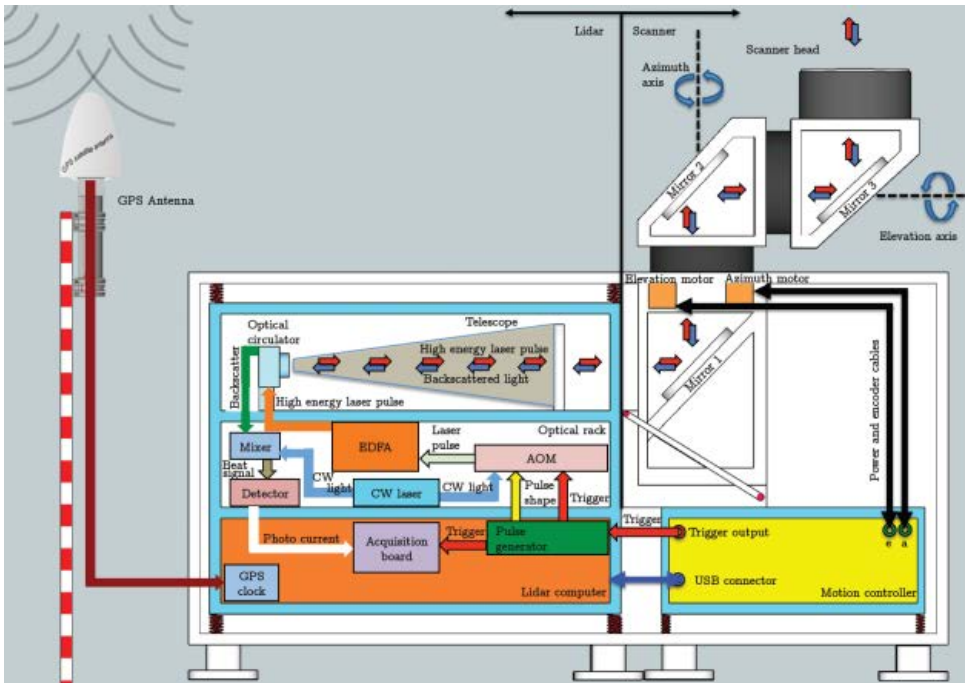

Figure 5: WindScanner internal hardware layout
Source: (Vasiljević, 2014)

The device specifications are further summarised in the table below:

Table 1: WindScanner device specifications

Scanner head motion	dual axis (azimuth + elevation)
Maximum speed, scanner head	50˚ /s [1]
Movement resolution	0.001° [1]
Trajectory Modes	PPI, RHI, LOS, DBS, and complex customised [1]
Laser source	Er-Yb silica fibre laser (pulsed) : PureSpectrum NLL [2]
Mean emission power	1 W [3]
Laser emission wavelength	1543 nm [3]
Telescope diameter	100 mm [3]
Pulse length	400 ns (long pulse), 200 ns (middle pulse) or 100 ns (short pulse) [1]
Pulse energy	100 µJ (long), 50 µJ (middle) or 25 µJ (short) [1]
Pulse repetition frequency	10 kHz (long), 20 kHz (middle) or 40 kHz (short) [1]
Photodetector sampling rate	4 ns (250 MHz) [3]

Eye safety	IEC/EN 60825-1 & ANSI-Z136.1-2007 compliant [3]
Maximum acquisition range	12 km [4]
Maximum normal operating range	6 km [4]
Maximum number of range gates	500 [1]
Radial wind speed range	-30 m/s to 30 m/s [4]
Accumulation time	100 ms (minimum), no maximum limit [1]
Dimensions	1.5 x 0.55 x 0.65 m [3]
Weight	150 kg [3]
Operating conditions	IP65 and ISO9227 compliant [3]

[1] = (Vasiljević, 2014), [2] = (Cariou et al., 2006), [3] = (Cariou et al., 2011), [4] = (Leosphere, 2013)

2.4.3 WindScanner Networking and Hardware Modifications

Beyond the commercially available Leosphere/DTU WindCube 200S, some key hardware and networking modifications have been made during development of the long range WindScanner system. These modifications are necessary to ensure proper coordination and synchronisation of a multi-LiDAR array.

As the WindScanner network is a unified and synchronised measurement system, each device must be linked through at minimum a LAN (local area network). It is preferable however if the devices are also outwardly connected to a WAN (wide area network), i.e. the internet. Since CAT-6 (Ethernet) cabling has a maximum length of 100m before signal degradation, a 3/4G mobile data modem is normally installed on each WindScanner. This allows for monitoring, control and data collection by the coordinating master computer. Further, each networked WindScanner is connected through a Cisco Meraki gateway (cloud based networking). This allows for remote management of individual and synchronised WindScanners from anywhere with an internet connection without the need for static addressing (only limited high cost options in mobile telecommunications currently exist).

One major issue faced during early prototyping was the asynchronous behaviour of commands and improper time stamps being recorded by the WindScanners. The system clock is based on a quartz oscillator with inherent and differing frequency errors. Factors such as temperature, humidity, and changes in supply voltage can affect the oscillation frequency of the crystal and cause a time drift between systems of typically 1PPM per ˚C and 10 PPM per day (1PPM = 0.0001%) (Windl, 2003). The WindScanner crystal clock oscillator has an accuracy of ± 50 ppm (Vasiljević, 2014). An error of this magnitude would result in a maximum lag of 720ms between devices after only 2 hours of operation. A maximum lag time of 10ms (100Hz) is considered acceptable for measurement coordination.

A solution of repeated direct synchronisation of each WindScanner clock was developed using Meinberg GPS (satellite) antennas with a precision of 250ns (Meinberg GmbH, 2015). Each WindScanner is equipped with a GPS antenna and when the time drift exceeds 10ms (monitored by the master computer), the correct time will be acquired and set within the system.

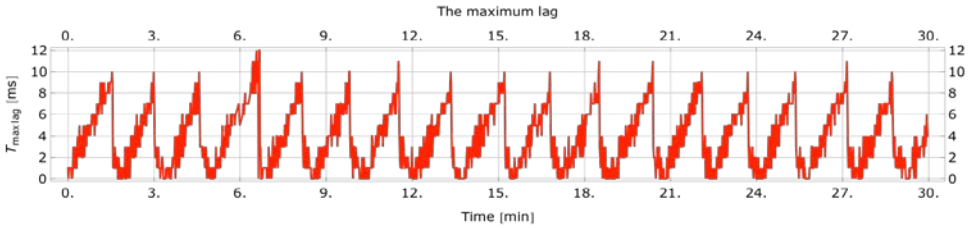

Figure 6: Effect of time synchronisation using GPS
Source: (Vasiljević et. al., 2013)

Another significant modification was the offloading of trigger signal control from the internal computer to the FPGA board and motion controller. This was done in order to optimise the pulse emission timing and position. In the original prototype, the computer would need to ask for and receive the scanner head position from the motion control unit before it could begin emitting pulses (resulting in a time lag). Now, the systems are integrated with a hardware connection between the motion control unit and FPGA board. This enables the pulse generator, AOM and acquisition board to begin operation exactly when the scanner head arrives at the precise position, with virtually no lag.

Further, the support structure of the scanner head from the early prototype was redesigned to more evenly distribute loads across all ranges of azimuth and elevation. The rear feet were moved closer together, and a stiff metal casing was designed which the scanner head sits atop of. This reduces the oscillation error from the scanner head movement, which acts to decrease the pointing accuracy of the system.

Lastly, the chassis grounding point was moved for lower electrical interference (noise) and an inclinometer was installed into a PCI-E RS-232 (serial) bus. This aids in calibration and levelling procedures, as well as monitoring shock to the devices. A digital humidity sensor was also added for protection and monitoring.

A much more detailed explanation of the end-to-end measurement process of the WindScanner system can be found in (Vasiljević, 2014).

2.4.4 WindScanner Software

Unlike the hardware adaptations, WindScanner software is not a modification of the WindCube equipped interface, but rather a completely separate entity. It is designed with the goal to be platform independent, and run on any commercial LiDAR with minimal modifications. The only shared components are the black box MLE (maximum likelihood estimation) routines which convert observed Doppler spectra into desired radial speed values.

The WindScanner software is separated into two components: MCS (Master Computer Software) and WCS (WindScanner Client Software), with communication between the two using the TCP/UDP protocol RSComPro. The RSComPro network architecture and packet data is presented in detail within: (Vasiljević et.al., 2013).

The WCS is run locally on each LiDAR computer, and controls the motion control, data acquisition, and storage functions of the single LiDAR unit.

The presiding MCS is run on any computer which is connected to the WindScanner device network (either locally or through Meraki routing). Live measurements as well as the device statuses can be viewed, and motion programs (including the CNR mapper) can be created and dispatched to the WindScanner clients. The master software also monitors the clock drift between clients and syncs them if necessary.

Figure 7: WindScanner Master Software in operation: Monitoring 3 synchronised WindScanner LiDARs

2.4.5 Site Deployment Procedures

In order to best ensure the highest quality measurements are taken, it is necessary to perform a regimented deployment on each WindScanner device every time the unit is moved. Issues particularly with shock and vibration during the transport process can misalign the scanner head and focus of the optical path leading to incorrect spatial referencing and low, or no backscatter signal.

The commercial WindCube 200S requires that the LiDAR be placed such that the home position (0 degrees azimuth, 0 degrees elevation) be facing north. With the long range WindScanners however, the device can be deployed in any direction, with the home position being offset by the angle relative to north.

After the WindScanner is placed on top of a fixed and steady platform (currently, in most cases a wooden pallet), the initial levelling process begins using the two bullseye bubble levels integrated into the outer casing. The device's adjustable feet are positioned in order to get an approximate level on both pitch and roll dimensions. Next, a higher precision digital level is used for fine adjustments. Lastly, the digital inclinometer which is fixed internally on the cage containing the optics and scanner head assembly is referenced to further verify that the system is indeed level.

Next begins the calibration of the scanner head positioning using a static "hard target" test. A hard target is an object which is non-transparent (opaque) and will subsequently not allow light (e.g. laser pulses) to pass through it. This results in a very high level of backscattering when a hard target is hit. Therefore, the CNR (carrier to noise ratio) value at the targeted distance and LOS reaches a maximum value. Common hard targets include: met-mast tips, booms and guy wires, radio antennas, surveying markers, building corners, etc.

DTU has incorporated an innovative visual technique for performing hard target calibrations, using the CNR mapper tool. A rough range of azimuth and elevation values (which contain the hard target position) are input into the CNR mapper program which runs within the master computer software. Tightly packed range gates (usually 1m separation) are set so as to also determine the precise distance from the WindScanner to the hard target. The area of chosen azimuth and elevation angles is scanned in stepwise PPI (constant elevation, varied azimuth) or RHI (constant azimuth, varied elevation) configurations, and a gradient of CNR dependent colours is generated for each distance (range gate). This "CNR map" can then be used to visually locate the hard target with high precision and verify that the scanner head positioning is correct. If there is any misalignment, then offsets within the motion control program can be adjusted.

An example of the CNR mapper output is given in the following figure. It depicts a met-mast at DTU Risø campus. The met-mast extension (boom) where the cup anemometer is mounted can be clearly seen.

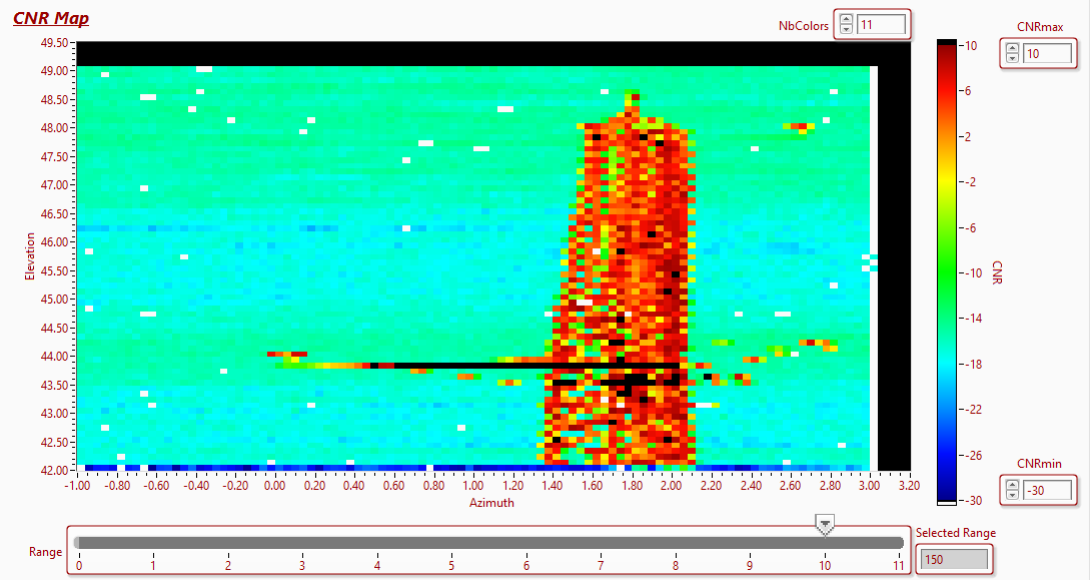

Figure 8: Example of CNR mapper scanning the top of a met-mast at DTU Risø campus

The standard procedure is to map multiple spatially separated hard targets in order to verify that the positioning is correct across all ranges which will occur during the scan. It is also good measure to periodically perform a hard target test during the campaign in order to verify that the pointing systems are operating normally.

3 Literature Review

3.1 LiDAR Validations

3.1.1 Dual Doppler

The use of Dual Doppler in remote sensing can be traced back to early weather radars, which were developed following WWII. Military radio operators experienced interference echoes from precipitation events, which led to the idea of using radio waves to detect meteorological phenomena (Bent, 1943). The first radar utilising the Doppler shift to calculate motion was developed in the 1950s at Cambridge University and was subsequently used to measure vertical motion within a rain shower (Barrat and Browne, 1953). (Brown and Peace Jr., 1968) reports the successful operation of the first dual Doppler experiment, which was also applied by (Browning et. al., 1968) to intersect a horizontal and vertical radar beam within a rain shower. (Lhermitte, 1970) further extended the measurement techniques of dual Doppler radar, which are used today throughout all remote sensing applications (including LiDAR).

(Newson et. al., 2015) performed a validation of the dual Doppler technique using the Halo Photonics Steam Line (a coherent scanning LiDAR similar to the WindCube 200S). Two LiDARs were positioned with four coordinated, intersecting RHI scans to form a grid surrounding a 60m met-mast. The perimeter (inflow and outflow areas) were then calculated using the dual Doppler velocity retrieval equations (which are presented in: Dual Doppler Velocity Retrieval) and compared to an in-situ ultrasonic anemometer mounted on the mast.

The experimental design with one instantaneous result is presented here:

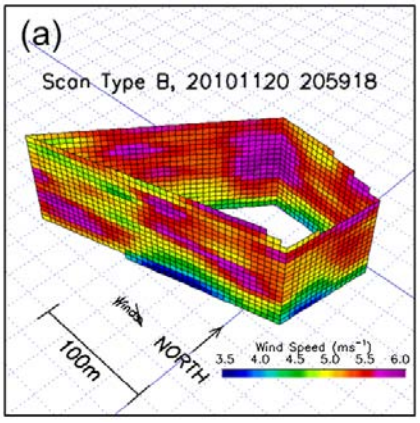

Figure 9: 3 dimensional visualisation at two instantaneous time periods of dual Doppler wind speed retrieval for scan type B
Source: (Newson et. al., 2005)

Their results show very good agreement between the dual Doppler LiDAR measurements, radar wind profiler and radiosonde, with all values agreeing within 3%. It was discovered that the (uncalibrated) ultrasonic anemometer was routinely over predicting the wind speeds by a factor of 14.2%. The results for wind direction were excellent, with a mean difference of 0.22 degrees.

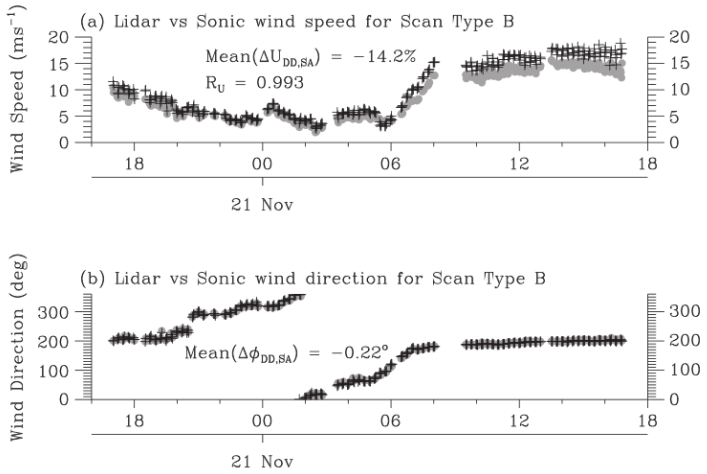

Figure 10: Comparison between dual Doppler LiDAR (grey circle) and ultrasonic anemometer (black +) at 60m for scan type B
Source: (Newson et. al., 2005)

3.1.2 Plan Position Indicator (PPI)

The PPI scan type also finds its beginnings in early Doppler radar. (Lhermitte and Atlas, 1961) first proposed a theoretical method of conically scanning a radar beam at a fixed elevation while varying the azimuth angle in full revolutions (VAD, or velocity azimuth display). When the beam sweeps through the incoming wind direction, the Doppler frequency (shift) reaches a maximum value. When the beam is facing away from the predominant wind direction, it is at its minimum. Thus, the data will form a sinusoidal curve, and the radial velocity can be displayed on a PPI scope (polar coordinate plot) for the given height. (Browning and Wexler, 1968) introduced and demonstrated the method with which wind speed and direction can be obtained from the amplitude and phase of the VAD measurements.

Later, it was proposed and demonstrated by (Schwiesow et. al., 1985) using a continuous wave LiDAR that a full conical scan might not be necessary, and that partial sector scans could be fit to the sinusoid curve using an iterative least squares approximation method. The results show very good agreement between the full scan (360˚) and half-scan (180˚) when sampling within a homogeneous atmosphere. The scatterplot is given below:

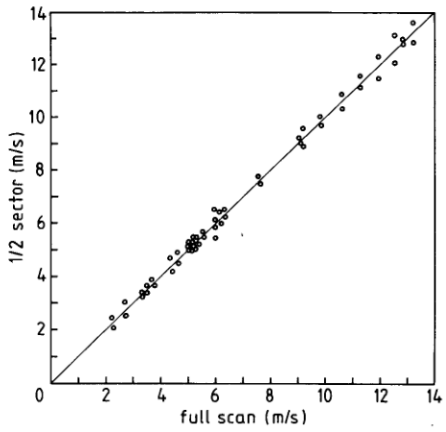

Figure 11: Wind speed comparison between 360˚ vs 180˚ VAD scan
Source: (Schwiesow et. al., 1985)

In more recent times, (Courtney et. al., 2014) used a Leosphere WindCube 200S to demonstrate the comparison between 30˚ and 45˚ sector scans, as well as the influence of two scanning speeds (2˚ and 3˚ /s) when compared to a reference cup anemometer (incidentally, the same mast and anemometer used in this study). The results also show good agreement with the reference, with deviations in the order of 3% for wind speed using 45˚ scans.

3.1.3 Long Range WindScanner System

Even though the WindScanner systems were only recently developed, a number of successful campaigns have been performed which demonstrate the robustness of the system and accuracy of the acquired measurements.

The first experiment, "Swinging Musketeer" was performed and detailed in the PhD thesis work by (Vasiljević, 2014). Three WindScanners were used in triple Doppler mode (all three beams intersecting) to measure the u, v and w components of the wind vector at three heights surrounding a met-mast. The results from the 76m scans show very good agreement with the ultrasonic anemometer and are shown below:

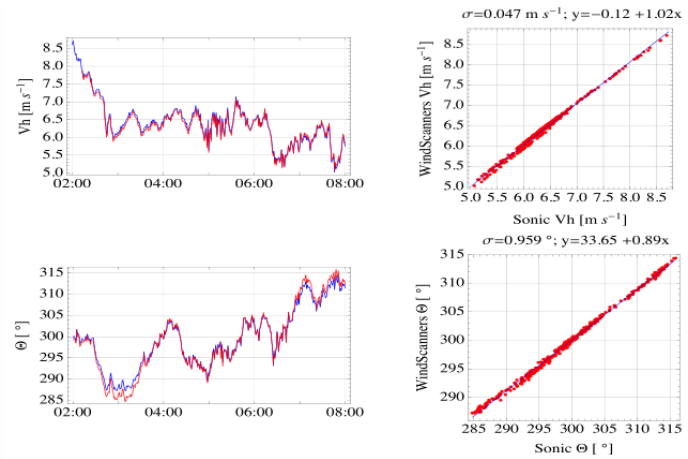

Figure 12: Results from the WindScanner "Swinging Musketeer" experiment
Source: (Vasiljević, 2014)

The second experiment to involve the long range WindScanners was also detailed in the thesis work of (Vasiljević, 2014). The IBL WiSH campaign reports a number of successful results:

- Identification of wind turbine wakes using surveillance scan PPI
- Determination of the boundary layer height and the presence of a low level jet using RHI scans
- Validation of radial speed measurements using triple Doppler configuration against an ultrasonic anemometer over a 9 hour period (results shown in the figure below)
- Synchronisation of three WindScanners on a complex trajectory to capture 3-dimensional flow
- Retrieval of the horizontal velocity distribution along a vertical plane

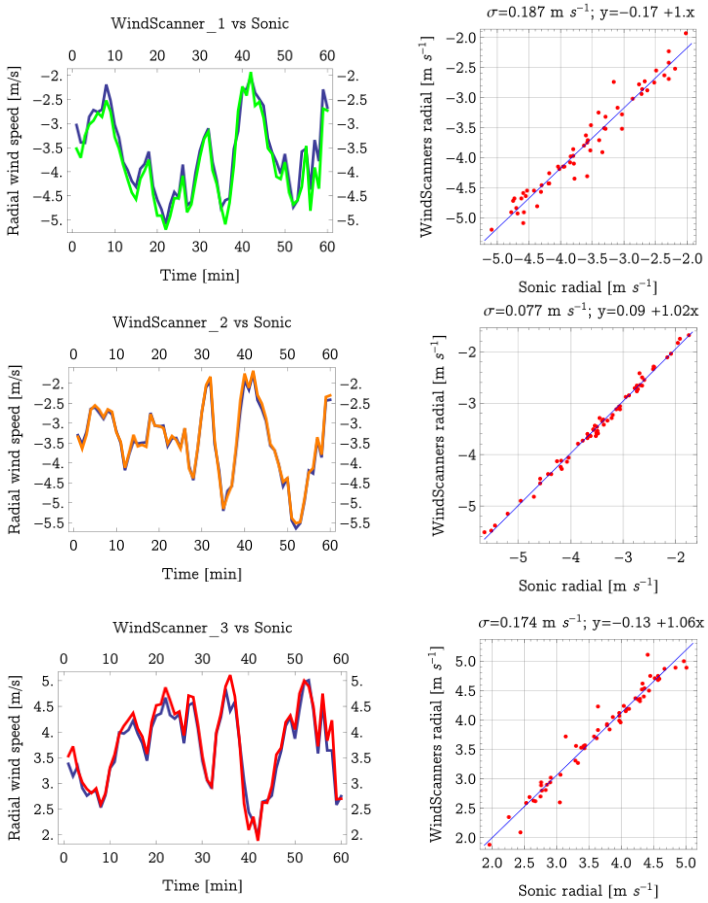

Figure 13: Comparison of 3 WindScanners to ultrasonic anemometer: 1 min averaged wind speed over 1 hour IBL WiSH experiment in Høvsøre, DK (Vasiljević, 2014)

Another recent experiment involving the WindScanner systems is the Kassel campaign in Germany. 6 long range WindScanners were deployed in Rödeserberg with the goal to obtain and validate measurements taken within complex, forested terrain. The results report proper operation of all systems, including excellent performance using mobile networking and a beam positioning error of 0.05˚. The systems obtained measurements within 1% of the mast mounted ultrasonic anemometers (Vasiljević, 2014).

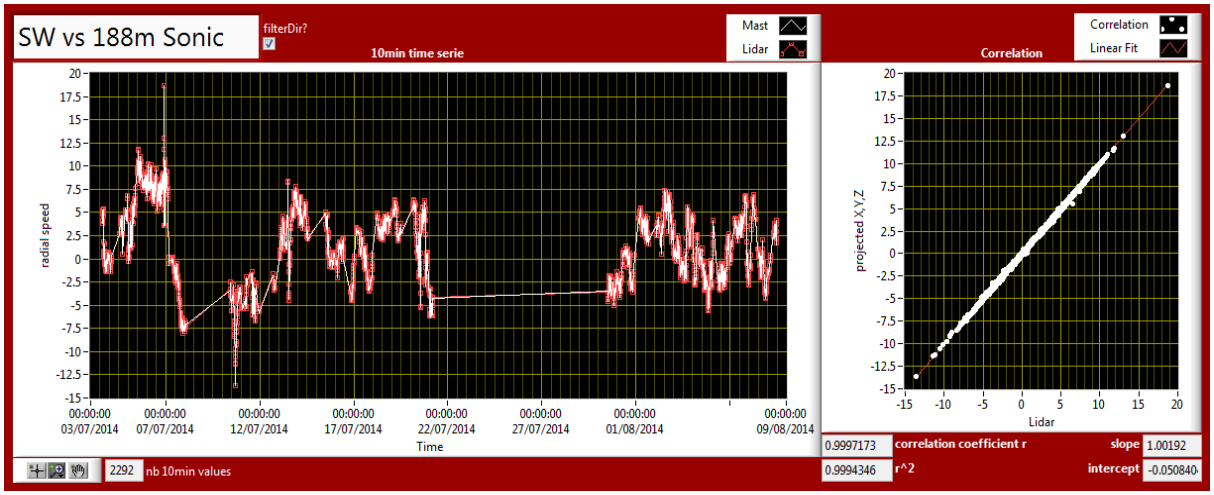

Figure 14: 10 minute averaged wind speed time series and correlation between WindScanner and sonic 188m anemometer in Kassel, Germany

Source: (Unpublished from internal report by Guillaume Léa, 2015)

4 Methodology

4.1 Introduction

The goal of this thesis is to determine the effect of a reduction in sector size against the ability for a scanning LiDAR to properly obtain wind speed and direction values. For this, some application specific software was created in order to handle all aspects of the analysis. This software (automated analysis software, or AAS) and the derived methodologies for data filtering and wind field reconstruction are presented in the following sections.

4.2 Data Filtering

It is necessary to perform some filtering on the raw data in order to obtain high quality output with which to perform the analysis. Filtering takes places in the following stages:

- CNR filter

High CNR values can represent the laser pulse interacting with a hard target, such as a turbine tower, mast structure/guy wires, etc. The difficulty in strict cut-off based CNR filtering is that factors such as aerosol concentration are changing over time and can influence the range of valid CNR values. It is usually apparent from visually comparing the time series graphs of CNR and radial speed over the scan which values are contaminated.
A suggested range of -25 to -5dB is usually appropriate, however in this analysis the filtering levels were decided visually (by the operator) within the AAS. A binary column 'filtered' is generated alongside the scan data, where a value of 1 represents a filtered LOS, and a 0 represents an unfiltered one. For the SSvsDD campaign, filtering based on both CNR and radial speed usually removes 0.3-2% of the values.

The entire raw and filtered graphs can be found in the link within: Appendix B: Raw Data.

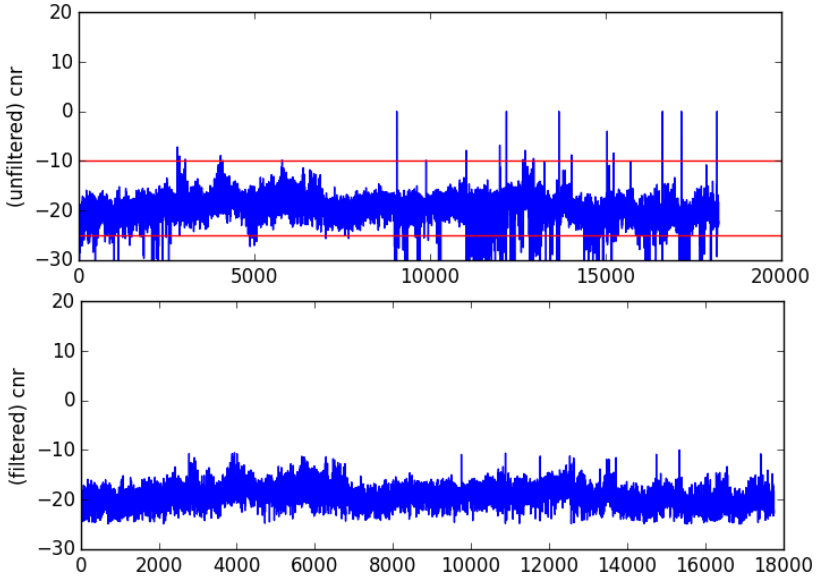

Figure 15: Example of CNR filtering (before and after)

∝ Radial speed filter

Often, filtering by CNR alone is not sufficient to remove all spurious LOS measurements from the dataset. This is because CNR filters which are too strict often remove excessive amounts of valid data points, while filters which are too lenient often leave erroneous values. Therefore, a combination of both CNR and radial speed filters was determined to be the best approach. Since radial speeds in a PPI configuration follow an oscillating (sine wave) pattern, it is also generally simple to find the cut off values by a visual inspection of the radial speed time series graph. Since the magnitude and sign vary depending on wind speed and LOS direction (towards or away from the LiDAR), it was decided to also determine cut-off limits by hand.

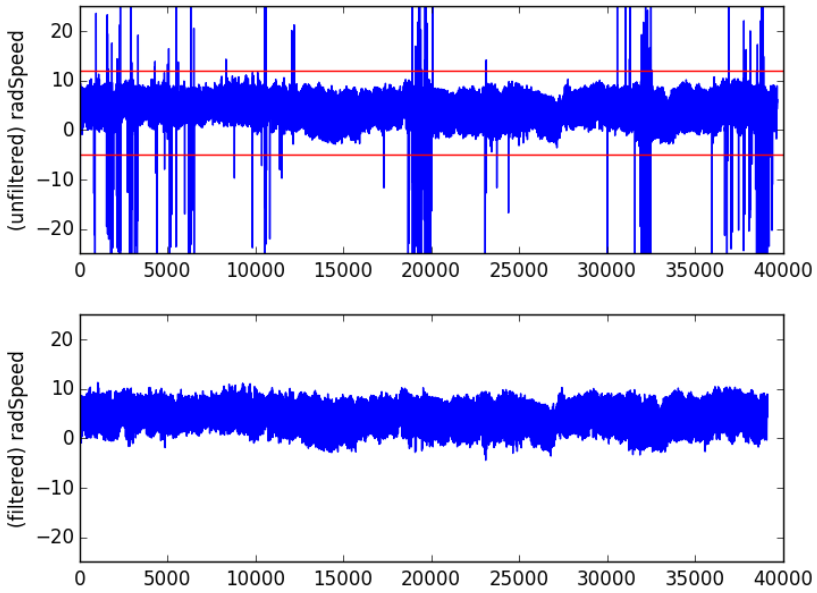

Figure 16: Example of radial speed filtering (before and after)

∝ Any partial scans (not all LOS) filter

After the previous filter functions (CNR and radial speed) have been run on every scenario, the reconstruction function (called 'fitting') breaks down (slices) the dataframe into n-sized smaller dataframes, with n being the number of LOS within the scan. In the SSvsDD dataset, this represents a length of 30 rows (60 degree sector size during measurement, with an azimuth separation of 2 degrees per LOS).

The fitting function then inspects the sliced dataframe containing one scan. If any of the LOS values have been filtered out, then the scan is discarded (NaN is written on all values for the scan time). Otherwise, the program continues on to the next step. Removing partially filtered scans is necessary in order to obtain the highest quality data with which to examine the effect of reconstruction using smaller sector sizes. In other cases such as normal measurement operation, this step may not be necessary. Typically, 2-20% of scans within each scenario are filtered out in the SSvsDD dataset.

∝ Reduction in sector size filter

Now that we have only full scans remaining with all available LOS radial speeds, the next step is to determine whether the program is being asked to reconstruct using a smaller sector size than the original measurement data (only for the purposes of this study). If so, then the scan is sliced once again into a smaller size of n-rows, where n is the number of LOS desired for the

given opening angle. For the case of a 30 degree sector reduction from SSvsDD, the new size will be 16 rows. This is due to a 2 degree separation between each LOS and the way the azimuth values are recorded in the data.

The middle LOS of the unfiltered scan is chosen, and half the new dataframe length is taken in both directions (so as to reduce the sector width symmetrically). In certain cases where the new length is an even number (so it is not possible to reduce the width symmetrically), then 1 additional LOS is included either on the left or right hand side at random.

∝ Waked wind direction and tower shadow effect filter

Due to the close proximity between the point of measurement (met-mast) and both wind turbines and other light/met mats at the Høvsøre site, it is necessary to perform some additional filtering to remove any possible wake (velocity deficit) or tower shadow effects from influencing the results of the study.

Using the simple Jensen linear wake model, it is possible to determine the range of wind directions from the turbines which need to be filtered. Although the Jensen model is not particularly accurate in near-wake zones, it provides a good first estimate which can be verified once the linear regression models are run.

$$D_W = D + 2kX$$

Where D_W = the diameter of the downstream turbine wake, D = the diameter of the turbine's rotor plane, k = the wake decay constant and X = the downstream distance.

Using a k value of 0.075 for flat terrain, we calculate the downstream wake diameter from the furthest turbine on stand #2:

$$D_W = (110m) + (2 * 0.075 * 1131m) \approx 280m$$

And the nearest turbine on stand #5:

$$D_W = (113m) + (2 * 0.075 * 185m) \approx 140m$$

Measuring out the respective wake diameters and removing sectors which could interfere with the measurement volume gives a wake free zone from 118-270 degrees. The tower shadow effect is determined to be fully encapsulated within the turbine wake volume. This result is further verified at the end of the study by plotting the absolute value of the difference between the LiDAR and reference wind speed against the direction given by the reference wind vane.

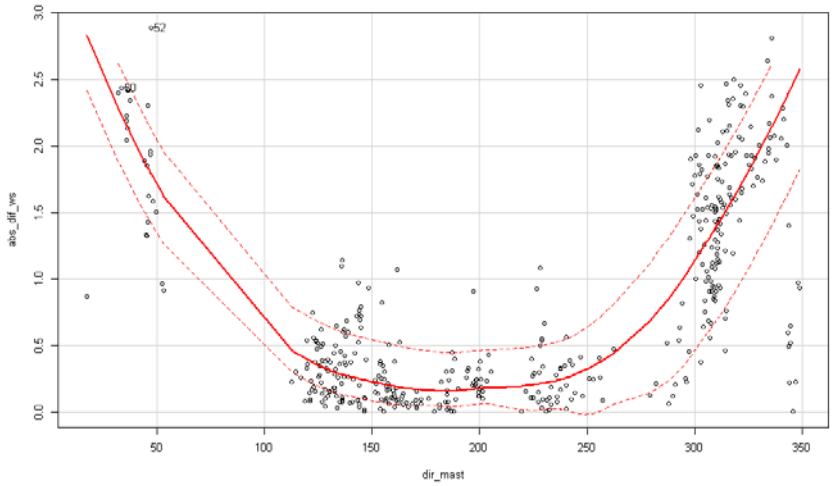

Figure 17: Verification of turbine wake effect from sectors outside 118-270 degrees

∝ Availability of scans within 10min average filter

When averaging data over a period of time, low number of samples and a non-uniform distribution of the samples can cause incorrect biasing within the averaged result. Therefore, a parameter is needed in order to determine how trustworthy the time averaged result is. During the resampling process of the analysis software written for this study, a column "avail" is calculated which contains the count of non-null values used to create the binned average. For the purposes of this dataset, we require that at minimum 19 samples (out of a maximum of 50) be available in order to trust the 10 minute averaged output. This is due to larger errors observed with less than 19 samples (38%) used in the averaging calculation.

∝ Wind speed between 4 and 25 m/s filter

For the purposes of the RUNE project, we are only interested in values which are within the operating range of a wind turbine. Therefore, we have chosen wind speed limits which closely resemble the cut-in and cut-out range of a modern utility scale wind turbine, such as the Siemens model SWT-2.3-93 (Siemens Wind Power, 2015).

Further, cup anemometers are notoriously prone to poor performance at low wind speeds. The wind tunnel calibration for this specific anemometer, performed by Deutsche WindGuard and attached in: Appendix E: Cup Anemometer Calibration , indicates a measurement uncertainty of 0.05 m/s at wind speeds of 4.085 m/s.

4.3 Reconstruction Algorithms

4.3.1 Wind Vector Components

Atmospheric (wind) flow is a 3 dimensional kinematic system and can be broken down into the vector components (u, v, and w). Remote sensing devices (e.g. LiDAR) can only measure the component of the wind velocity which is parallel to the LOS beam. Therefore, the radial velocity which is measured is actually the projection of the true wind speed on the laser's line of sight.

The magnitude of the wind components projected along the radial LOS in the zero degree elevation case is given by:

$$rs\ (m/s)\ = ws\ * \cos\theta$$

Where ws represents the true wind speed and θ represents the angle between the wind direction and the radial LOS.

When the wind direction is aligned with the radial LOS such that (θ = 0 or 180˚), the radial velocity will represent the true (or negated) wind speed. For cases where the wind direction is perpendicular (θ = 90 or 270˚) such that cos θ = 0, there will be no component projected along the LOS, and the LiDAR will be unable to measure any portion of the wind.

When extending the equations to scenarios which include an elevation angle higher than zero, these components together form the radial speed (rs) vector through:

$$rs\ (m/s) = \ u\cos(\theta)\cos(\varphi) + v\sin(\theta)\cos(\varphi) + w\sin(\varphi)$$

Where θ represents the azimuth angle, and φ represents the elevation angle (altitude).

Component u represents the zonal velocity along the east-west axis.

Component v represents the meridional velocity along the north-south axis.

Component w represents the vertical velocity. In this analysis we disregard the vertical wind component (see section 4.3.2 for more information on this).

Knowing the true wind speed and direction, it is simple to obtain u and v components in the following way:

$$u = ws * \cos(dir)$$
$$v = ws * \sin(dir)$$

In order to work backwards and obtain the familiar scalar horizontal wind speed value (expressed in m/s), we calculate the magnitude of the u and v components using the Pythagorean Theorem:

$$horizontal\ ws = \frac{\sqrt{u^2 + v^2}}{\cos\varphi}$$

Lastly, the wind direction is obtained using the two argument inverse tangent function (atan2). This is due to necessary inputs on the component signs (+/-) and limitations with the single argument (arctangent) function returning undefined values when u = 0.

$$dir\ (degrees) = atan2(u, v) * \frac{180}{\pi}$$

It is important to note that the direction result is expressed in mathematical terms (Northerly = 360 or 0˚, Easterly = 90˚, Southerly = 180˚ and Westerly = 270˚) instead of meteorological terms where (Northerly = 270˚, Easterly = 180˚, Southerly = 90˚ and Westerly = 0 or 360˚). A detailed explanation of coordinate system standards can be found in (Long, 1994).

4.3.2 Assumptions

In sector scan campaigns, we utilise low elevation angles such that we regard $\sin\varphi = 0$ and disregard the vertical component w in our equations. It is possible to obtain the vertical component (w) using dual Doppler measurements by first assuming w = 0 as a surface condition and then iterating the continuity equation:

$$(\rho w)_b - (\rho w)_a = -\left[\rho\left(\frac{\partial u}{\partial x}+\frac{\partial v}{\partial y}\right)_b \Delta z - \rho\left(\frac{\partial u}{\partial x}+\frac{\partial v}{\partial y}\right)_a \Delta z\right].$$

Until the mean difference between horizontal and vertical results approach some very small limit. A full derivation of this principle can be found in the appendix of (Huddleston, 2012). Using three of more LiDARs (i.e. triple Doppler), it is possible to directly measure all three vector components (u, v and w) from a single point in space with no assumptions.

Since sector scanning requires LOS measurements over a distributed area in order to reconstruct wind speed and direction, we must also make the assumption that the horizontal flow over the entire scanned area is homogeneous. The effect of this assumption will vary depending on sector size, complexity of flow, atmospheric stability, turbulence, etc. More background on this is presented in the next section.

4.3.3 Sector Scan (PPI) Reconstruction

There are numerous methods to reconstruct horizontal wind speed and direction from radial LOS measurements in a single Doppler PPI scenario. The core idea is that for a single LiDAR to obtain estimations for u and v, multiple spatially separated points must be sampled. This is because at minimum, two radial speed measurements are necessary to obtain estimates of u and v.

Two main approaches exist for PPI reconstruction: Variational Assimilation (mathematical minimisation of an error/cost function to produce lowest expected variances), and simple statistical/geometric fitting, such as VAD or Velocity Azimuth Processing (VAP). We will employ the simplified models in this analysis.

The simplest approach for PPI scans less than 360 degrees is to use the integrated, or extended VAD reconstruction algorithm. Radial speed data is point processed to fit to a sinusoidal curve. The fitted function then has the representative properties: amplitude = wind speed, phase = wind direction, and offset = vertical velocity (Browning, 1968).

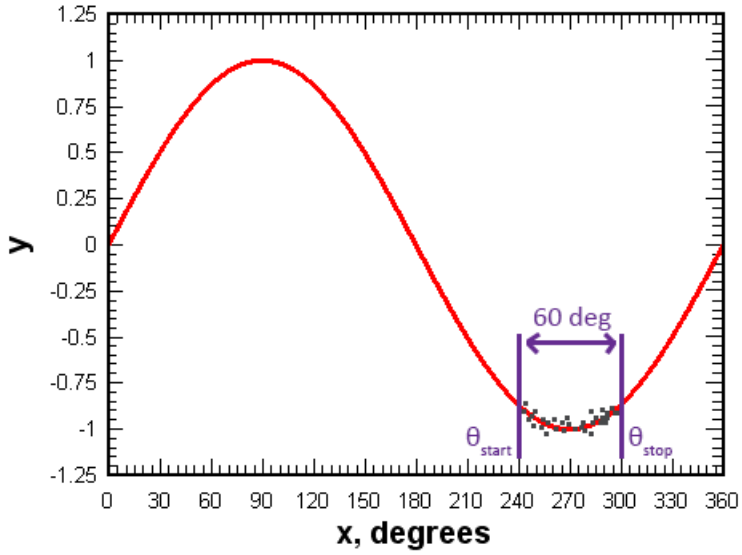

Figure 18: Point process fitting of radial speed values to sine function from 60˚ sector scan

The highest or lowest point of the sine wave's amplitude represents the best fitting area, as it provides the most distinctive shape within the curve with which to match. Therefore the reconstruction algorithm results in the lowest measurement error at the peak and base of the fitted trigonometric function.

As a reminder from what was mentioned in: Assumptions, the horizontal wind conditions (e.g. speed, direction and composition) over the scanned area must be considered uniform in order to solve the equations.

The simplest VAP approach only takes into account the start and end measurement points of the scanned arc. The points are fit to a sine curve using a trigonometric least squares regression, in which the residuals of the fitted points are minimised.

$$\overline{u} = \frac{V_{\theta_1} \sin\theta_1 - V_{\theta_2} \sin\theta_2}{\sin(\theta_1 - \theta_2)}$$

$$\overline{v} = \frac{V_{\theta_1} \cos\theta_1 - V_{\theta_2} \cos\theta_2}{\sin(\theta_1 - \theta_2)}$$

An improvement on this simplified model is extending the formula to include measurements over the entire scanned area (i.e. integrating the elements from the start to stop azimuth range). In practice, this results in a summation of the angularly separated LOS velocities. The formulas for obtaining u and v estimates using the integrated VAP method are given below:

$$\bar{u} = \frac{(\sum_{\theta_{start}}^{\theta_{stop}} (rs * \cos\theta) * \sum_{\theta_{start}}^{\theta_{stop}} (\sin^2\theta)) - (\sum_{\theta_{start}}^{\theta_{stop}} (rs * \sin\theta) * \sum_{\theta_{start}}^{\theta_{stop}} (\cos\theta * \sin\theta))}{((\sum_{\theta_{start}}^{\theta_{stop}} \cos^2\theta) * \sum_{\theta_{start}}^{\theta_{stop}} \sin^2\theta)) - (\sum_{\theta_{start}}^{\theta_{stop}} (\cos\theta * \sin\theta))^2)}$$

$$\bar{v} = \frac{(\sum_{\theta_{start}}^{\theta_{stop}} (rs * \sin\theta) * \sum_{\theta_{start}}^{\theta_{stop}} (\cos^2\theta)) - (\sum_{\theta_{start}}^{\theta_{stop}} (rs * \cos\theta) * \sum_{\theta_{start}}^{\theta_{stop}} (\cos\theta * \sin\theta))}{((\sum_{\theta_{start}}^{\theta_{stop}} \cos^2\theta) * \sum_{\theta_{start}}^{\theta_{stop}} \sin^2\theta)) - (\sum_{\theta_{start}}^{\theta_{stop}} (\cos\theta * \sin\theta))^2)}$$

Once estimates for u and v are calculated, it is simple to calculate the horizontal wind speed and direction using the formulas presented in section: 4.3.1.

4.3.4 Dual Doppler Velocity Retrieval

The dual Doppler retrieval algorithm used in the analysis is as follows:

For each LiDAR index *i* (#1 or 2), the radial speed measurement u_{ri} can be used to obtain estimations of the vector components (*u, v, w*) of the wind speed.

$$u_{ri} = u \sin\theta_i \cos\varphi_i + v \cos\theta_i \cos\varphi_i + w \sin\varphi_i$$

Where θ represents the azimuth angle and φ represents the elevation angle of each respective LiDAR.

Since the elevation angles used in the experiment are sufficiently small, we can assume that the vertical component w does not contribute to the observed radial speed vector and discard it. The formulas for obtaining u and v estimates are given from (Newsom, 2015):

$$u = \frac{\hat{u}_{r1} \cos\theta_2 \cos\varphi_2 - \hat{u}_{r2} \cos\theta_1 \cos\varphi_1}{\cos\varphi_1 \cos\varphi_2 \ (\sin\theta_1 \cos\theta_2 - \sin\theta_2 \cos\theta_1)}$$

and

$$v = \frac{\hat{u}_{r2} \sin\theta_1 \cos\varphi_1 - \hat{u}_{r1} \sin\theta_2 \cos\varphi_2}{\cos\varphi_1 \cos\varphi_2 \ (\sin\theta_1 \cos\theta_2 - \sin\theta_2 \cos\theta_1)}$$

Once solutions for u and v are obtained, they can be combined using the same approach for sector scan reconstruction to obtain the horizontal wind speed and direction.

4.4 Overview of Automated Analysis Software (AAS)

A centralised and automated application was developed during the course of this thesis which handles the entire sector scan and dual Doppler analysis workflow. It is written in Python (version 3.4.3) and is released open source under the Creative Commons Attribution-ShareAlike 4.0 International License (Creative Commons, 2015). The data structure used is the pandas DataFrame, which is a 2-dimensional array similar to NumPy's ndarray. The pandas library was chosen due to its integrated indexing, quick searching, subsetting and grouping, and time series functionality. Plotting functions are handled by matplotlib.

4.5 Analysis Workflow

4.5.1 Software Architecture

The AAS was written using object oriented design and is well documented. A flowchart is presented showing the high level processes:

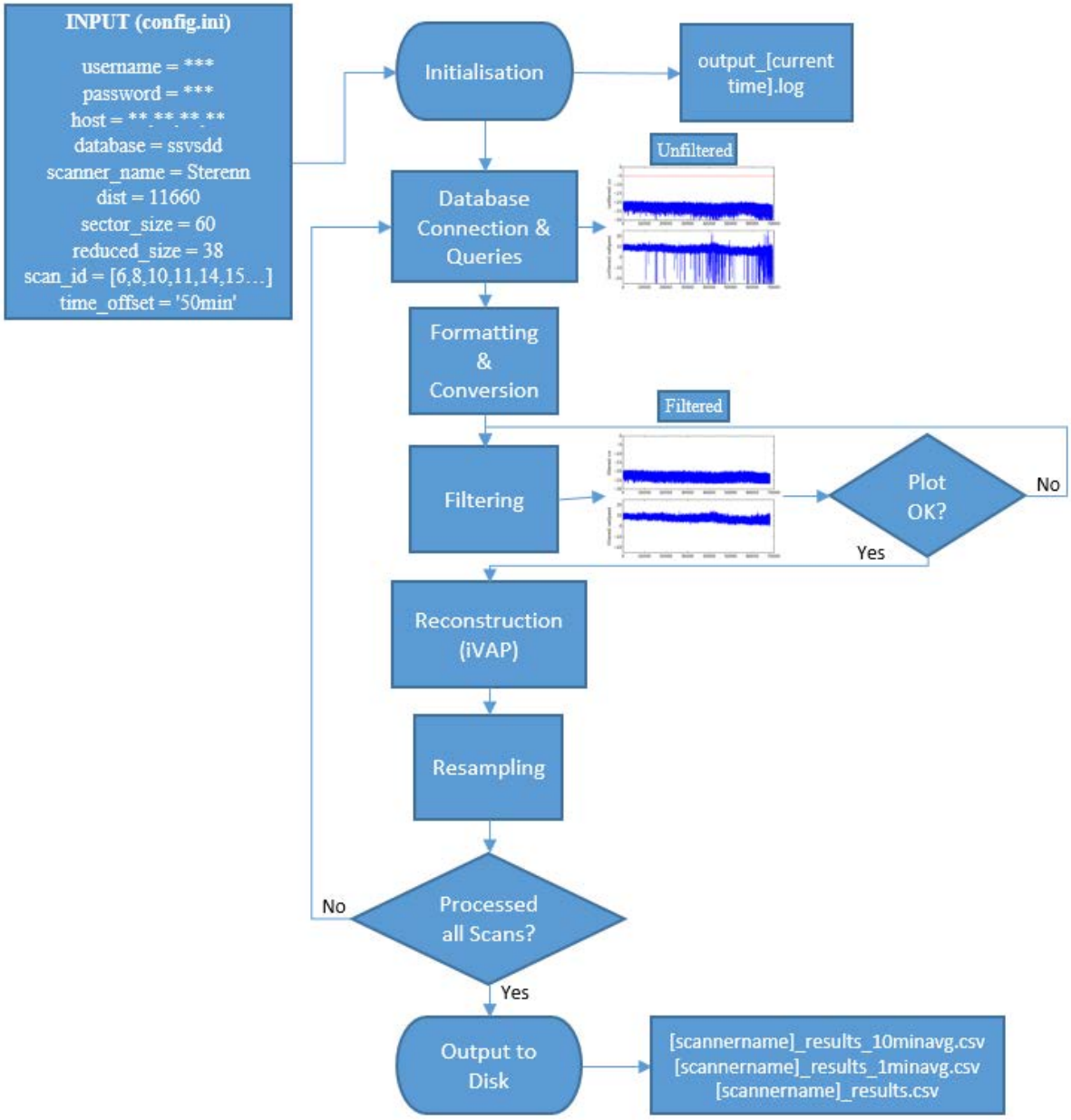

Figure 19: Automated Analysis Software (AAS) architecture flowchart

The steps are further explained in the following list:

- Initialisation:
  Loads config.ini file, which contains campaign specific data. Ex. MySQL database configuration, range gate (distance) for analysis, sector size, list of scan ids, time offset, CNR and radial speed filter limits. Also sets up logging object and records to .log file
- Database connection & queries:
  Loops through the list of scan ids, specifying SQL queries and fetching data
- Formatting & conversion:
  Fix azimuth stamps, join necessary columns
- Filtering:

If ranges are provided, apply filters for CNR and radial speed. Otherwise plot unfiltered data and prompt for limits before filtering

- Plotting:
  Plot the filtered data and ask for user approval. If not approved, return to previous step and prompt for new filters
- Reconstruction:
  Slice data into n-length scans (n= number LOS) and apply iVAP equations to calculate u, v and subsequently horizontal speed and direction
- Resampling:
  Resample fast data into 1 and 10 minute averages, with the time stamped at the end of the period. Apply a time shift if provided. Also count the number of non-NaN values and place in a column called 'avail'. Append the results for this scan id to the master results dataframes
- Processed all scans?
  If there are any scan ids remaining, loop back to acquiring data
- Output to disk:
  Write the master results dataframes (fast, 1min, 10min) to a .csv file and save the results plots to the hard drive. Exit the program successfully

5 Data Acquisition: Høvsøre SSvsDD Campaign

5.1 Preface

Initially, this thesis began with investigating the measurement data taken during the wisscas campaign (WindScanner Site Calibration Assessment for Siemens) in January 2014 at the Høvsøre test station. This was part of a larger experiment which was ended by a lightning strike which disabled many of the reference instruments. The WindScanners were updated to measure above a different met-mast which is operated by Vestas. However, a series of limitations arose during the analysis which diminished the scientific quality of the study. Mainly:

- Wind vane was taken offline for maintenance (direction values could not be collocated)
- Data was only stored for 10 minute averages
- Icing potential (cup anemometer operating outside of calibration limits)
- Unusual climate conditions (winds from East)
- Significant wake interference from the turbines due to the unusual wind direction

Therefore, it was chosen to switch to the SSvsDD dataset instead, which increased significantly the quality and confidence of the results.
A small study from the wisscas data, which investigates the possibility of extracting "simulated" dual Doppler measurements from two LiDARs performing sector scans is presented in: Appendix F: .

5.2 Overview

The Sector Scan vs. Dual Doppler (SSvsDD) experiment was initiated in order to test the performance of two WindScanners in dual Doppler mode against one WindScanner in sector scan mode. The main commercial purpose of the study is to determine whether two WindScanners in dual Doppler mode are actually needed in order to accurately measure wind speed and direction for the purpose of resource assessment and wind farm site optimisation. Utilising only one WindScanner in sector scan mode allows for a reduction in project costs as well as the opportunity to increase measurement area by dedicating the second WindScanner to another purpose.

The campaign took place from April 30, 2014 until May 7, 2014 at DTU's test centre in Høvsøre, Denmark. Three WindScanners were deployed, with two configured in a fixed, staring LOS configuration (dual Doppler), while the other was performing 60 degree sector scans. The middle LOS of the sector scan intersected with the dual Doppler beams directly above a cup anemometer on the site's southern 116.5m met-mast. This allows for a comprehensive comparison between the three measurement approaches, which will be presented within the results and conclusion section.

5.3 Location

Measurement data used in this experiment was collected at the Danish National Test Centre for Large Wind Turbines at Høvsøre, on the Western coast of the Jutland peninsula in Western Denmark. The site is administered by DTU Wind Energy, with offices located at: Bøvlingvej 41B 7650 Bøvlingbjerg, DK (UTM: 32V, 447901.40 m E, 6256574.19 m N).

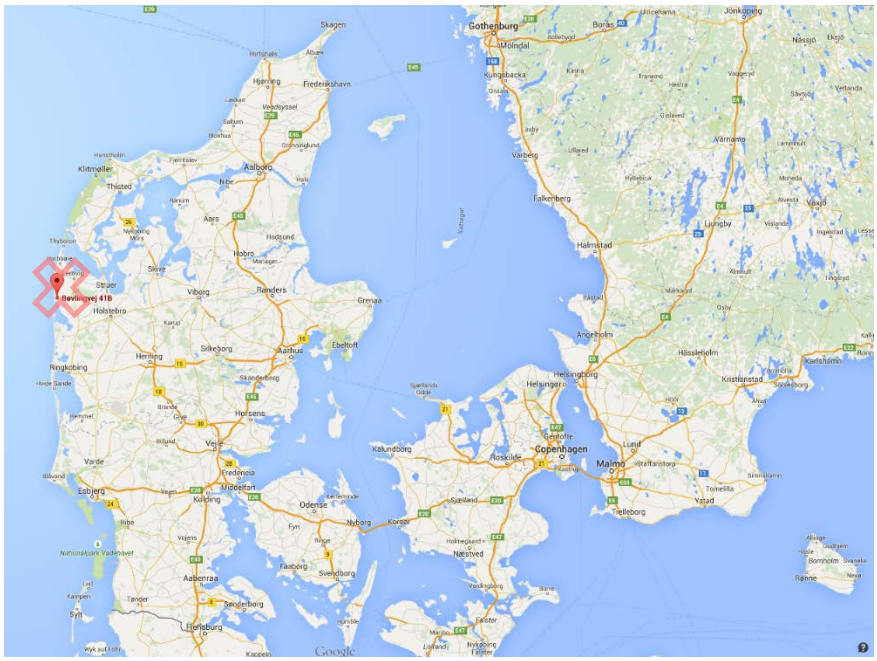

Figure 20: Location overview of Høvsøre Test Station
Source: Modified from (Google Maps web, 2015)

The site was chosen for its extensive instrumentation, technician support, and history of validated and published literature which will be referred to in the review section. This helps to minimise the amount of unforeseen parameters which can affect the results of the study.

The Høvsøre site consist of flat, simple terrain with only small elevation changes nearby. The maximum elevation is 3m (max slope 2.6%) and minimum -1m (min slope -2.5%). Met mast #6 lies at 0m elevation and 0% slope.

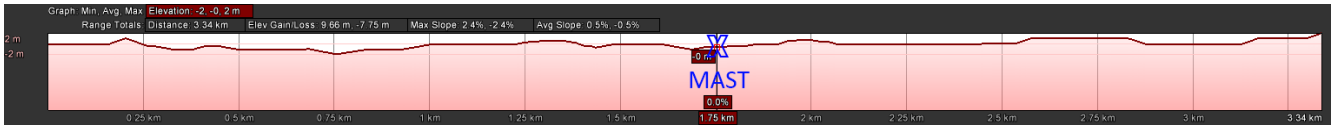

Figure 21: Elevation profile 1.5 km east and west of the met-mast
Source: Modified from (Google Earth, 2015)

Directly west of the site (1.45 – 2km) lies the North Sea. At the coastline, there is a small dune running parallel to the shore with maximum elevation of 3m (min 0m) and maximum slope of 3% (min -3.8%). The maximum height occurs directly west of met-mast #3 (at 260 degrees to met-mast #6).

Figure 22: Elevation profile of coastline (2km parallel to Høvsøre site)
Source: Modified from (Google Earth, 2015)

5.4 Layout

The Høvsøre test site consists of 5 turbine stands, each with a respective met-mast located directly west. There is also a tall met-mast (116.5m) located at the south end of the site near the LiDAR calibration pad. Additionally, there are two 160m aircraft warning light towers to the east of the north & south turbine stands. Each structure is shown below in the site layout overview.

Figure 23: Overview of site layout
Source: Modified from (Google Earth, 2015)

Three WindScanners were deployed within the campaign. Two devices (WS_K: Košava and WS_W: Whittle) were set-up in dual Doppler mode, with a 63 degree opening angle intersecting just above the southernmost met-mast. The other (WS_S: Sterenn) was configured in 60 degree sector scan mode, with the middle line of sight collocated both with the dual Doppler beams and also a cup anemometer mounted on top of the 116.5m met-mast. The wind direction is taken from a wind vane mounted at 100m on the same tower. The campaign specific layout can be seen in the following figure:

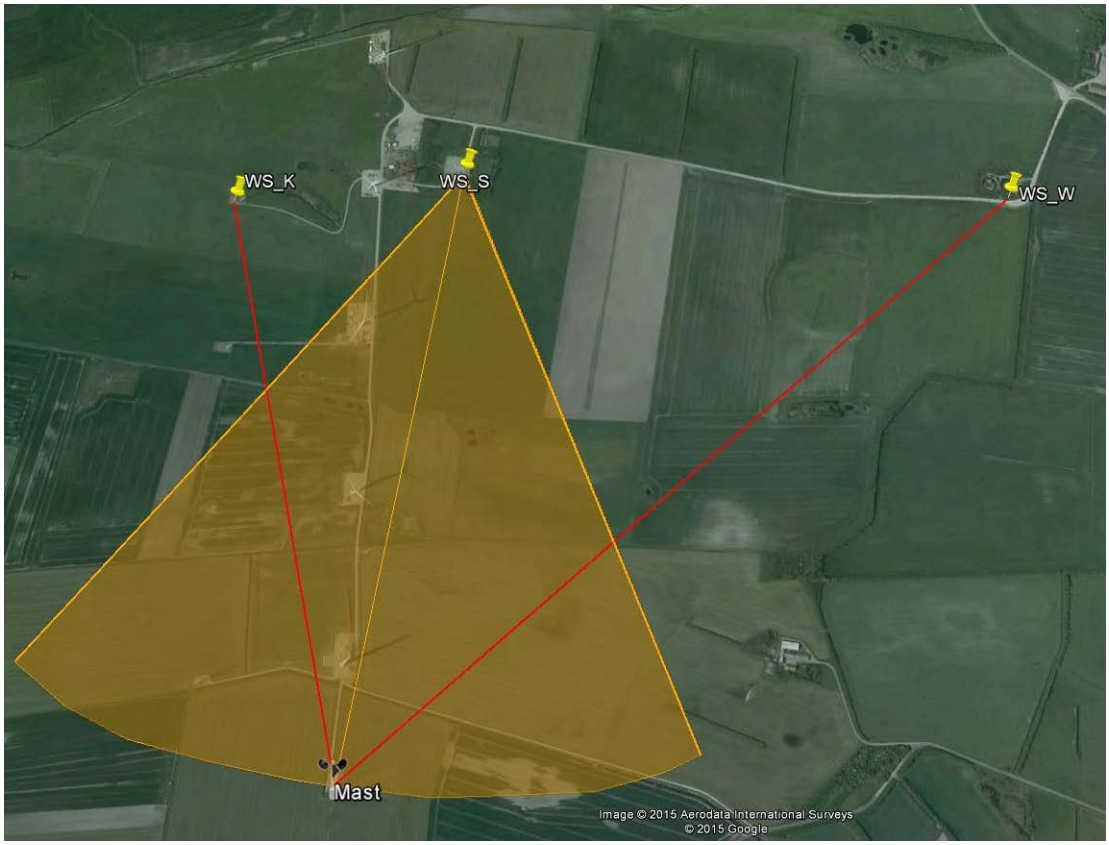

Figure 24: Overview of campaign layout
Source: Modified from (Google Earth, 2015)

Geospatial coordinates for the devices were measured using differential GPS with an accuracy of 10cm. The results are presented in the following table (UTM system, Zone 32V):

Table 2: SSvsDD deployment positions

Object	Easting (m)	Northing (m)	Height (m)	Elevation Angle (degrees)
WS_K	447450.548	6256541.135	4.054	6.1
WS_S	447893.983	6256558.133	5.078	5.96
WS_W	448937.717	6256404.894	5.409	4.25
116.5m Met-Mast (base)	447647.39	6255435.76	4.836	N/A

Because turbine manufacturers are constantly replacing and modifying their installations at Høvsøre, the following table will document the site's status during the experiment. It is important to note that there was no turbine installed on stand #1 during the measurement period.

Table 3: Turbine specifications at Høvsøre
Source: (DTU Wind Energy, 2015)

Stand	Company	Model	Power (MW)	Rotor Diameter	Hub Height	Tip Height
1	NONE	NONE	NONE	NONE	NONE	NONE
2	Vestas	V90-2.0MW	2.0	90	84	129
3	Siemens	SWT 4.0/130	4.0	130	95	160
4	Nordex	N100-3.3	3.3	100	75	125
5	Siemens	SWT 3.0-113	3.0	113	99,5	156

5.5 Measurement Scenario

5.5.1 Hard Target Mapping

The general approach outlined in: Site Deployment Procedures was followed before any measurements were taken. The CNR mapper output is presented in the following figures to validate that the devices were functioning normally and that the correct azimuth, elevation and range gates were used in the analysis.

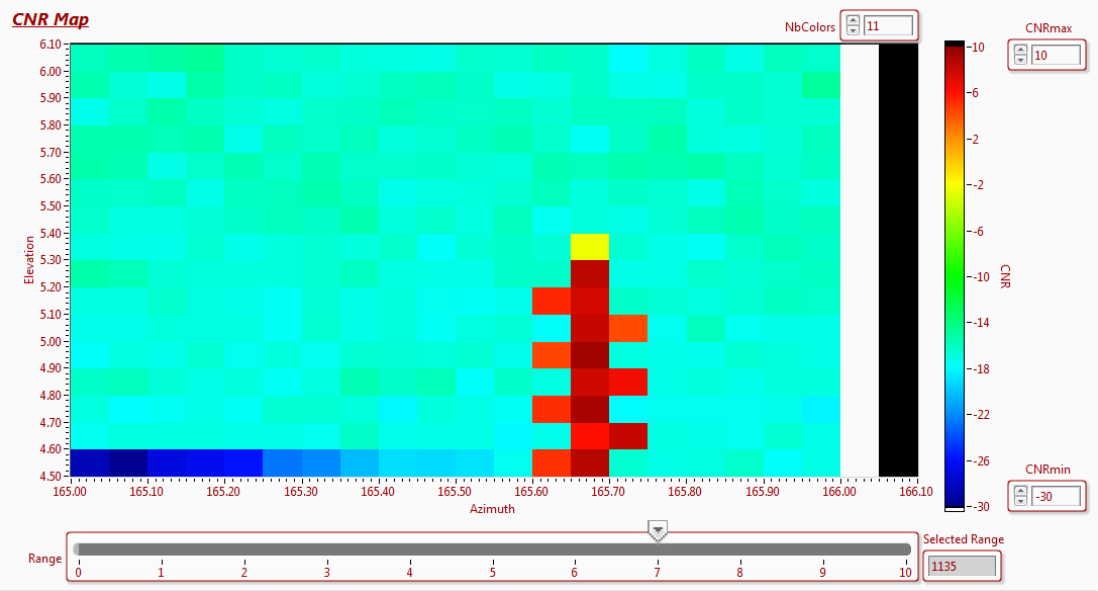

Figure 25: CNR Mapper results: Košava

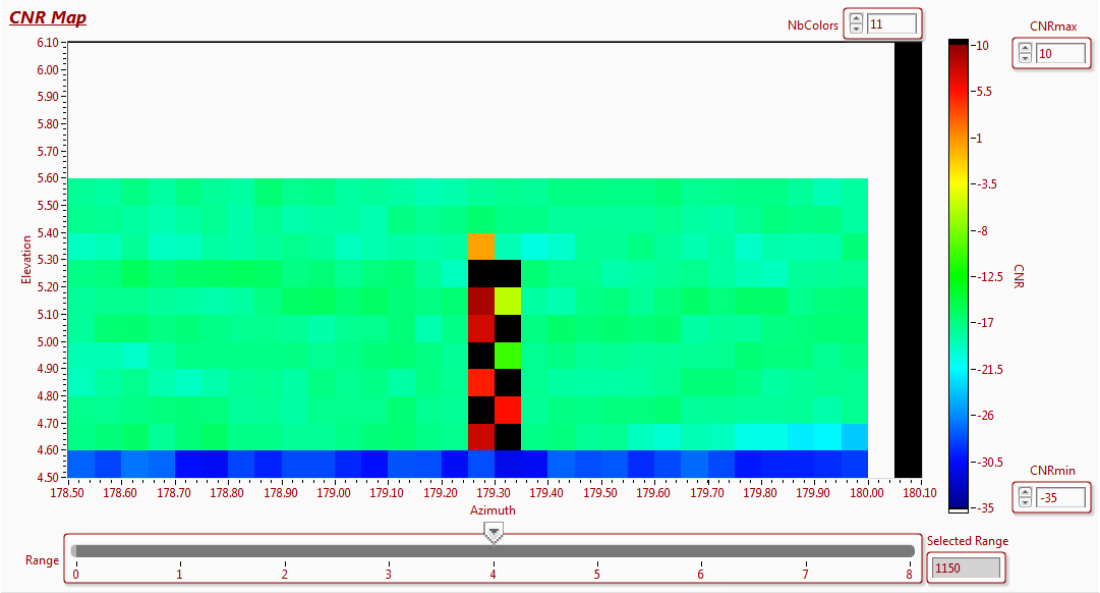

Figure 26: CNR Mapper results: Sterenn

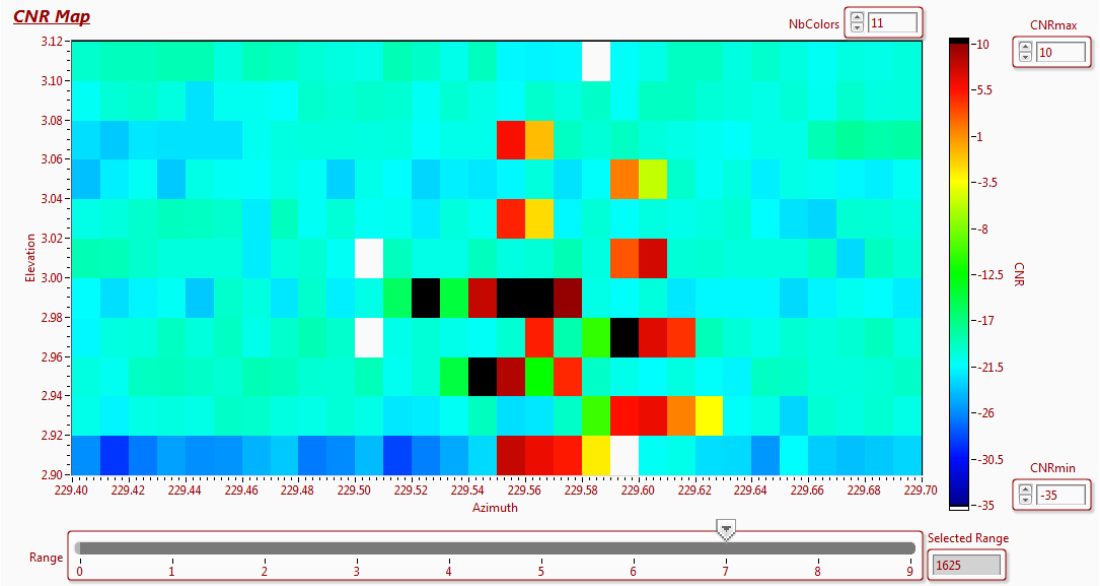

Figure 27: CNR Mapper results: Whittle

5.5.2 WindScanner #1: Sterenn

Table 4: WindScanner configuration: Sterenn

WindScanner Sterenn : Property	Value
Scan type:	PPI (sector scan)
Sector size:	60 degrees
Elevation angle (φ):	5.36 degrees
Elevation offset:	0.6 degrees
Azimuth range (θ_{Start} : θ_{Stop}):	150.xxx : 208.xxx (auto-reversing)
Azimuth offset:	12.31 degrees
Linear distance:	1149.14 m
Range gate to cup:	1166 m (41 range gates in total)

Position (UTM):	{447893.983m E, 6256558.133 m N, 5.078 m Height}
Scanning speed:	2.5 degrees / s
Time per scan:	12 s
Azimuth separation:	2 degrees per LOS (30 LOS)
Pulse length:	200 ns
Accumulation time:	400 ms
FFT size:	64

We find linear distances between the WindScanners and the base of the met-mast using the Euclidian distance approximation:

$$distance = \sqrt{(E_1 - E_2)^2 + (N_1 - N_2)^2 + (H_1 - H_2)^2}$$

Where E_i and N_i represent the Easting and Northing components of the UTM coordinates and H_i represents the object's altitude above sea level (ASL).

Line of sight distances between the WindScanners and the cup anemometer are then calculated using the same formula, considering to aim above the cup anemometer (to avoid potential hard target contamination).

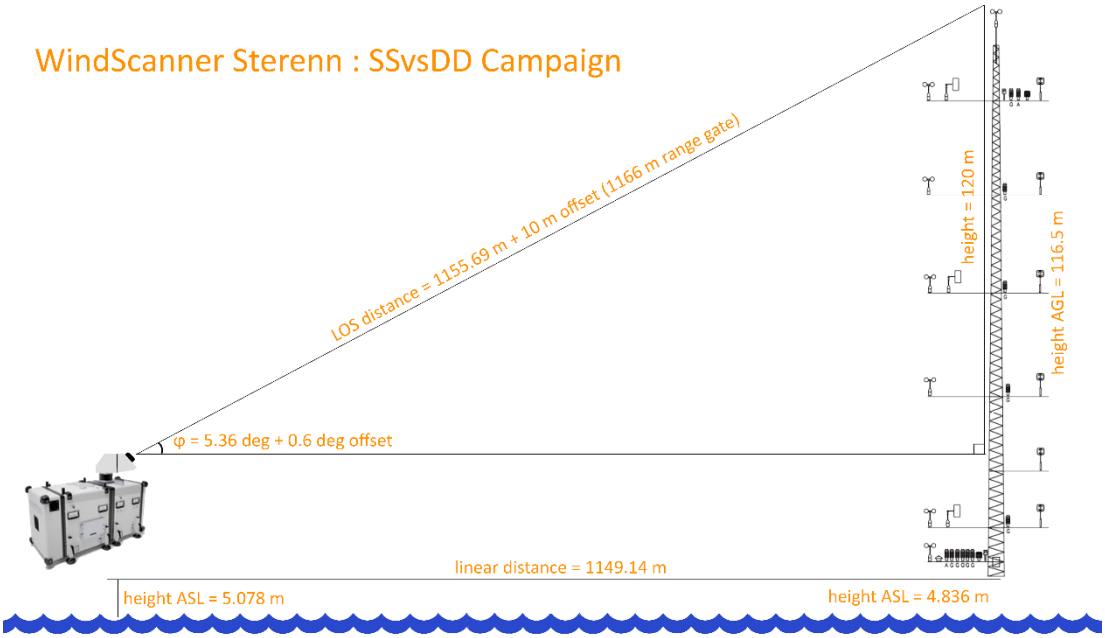

Figure 28: Sterenn measurement geometry

5.5.3 WindScanner #2: Košava

Table 5: WindScanner configuration: Košava

WindScanner Koshava : Property	Value
Scan type:	Fixed LOS (dual Doppler with Whittle)
Elevation angle (φ):	5.32 degrees
Elevation offset:	0.78 degrees
Azimuth angle (θ):	165.66 degrees
Azimuth offset:	3.46 degrees

Linear distance:	1122.76 m
Range gate to cup:	1135 m (41 range gates in total)
Position (UTM):	{447450.548, 6256541.135, 4.054}
Pulse length:	200 ns
Accumulation time:	500 ms
FFT size:	64

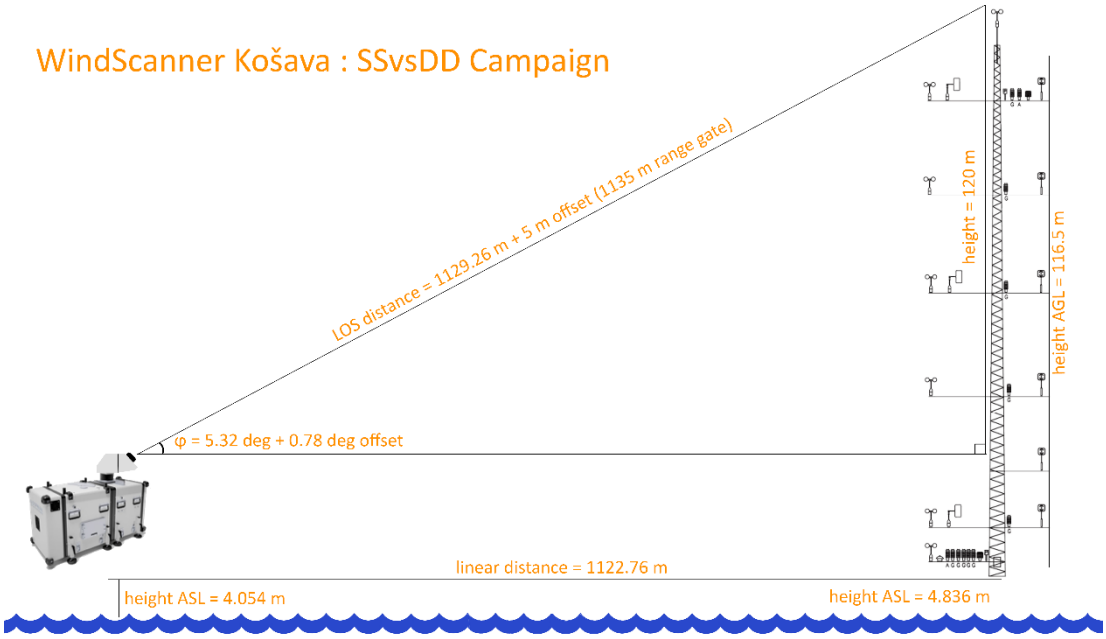

Figure 29: Košava measurement geometry

5.5.4 WindScanner #3: Whittle

Table 6: WindScanner configuration: Whittle

WindScanner Whittle : Property	Value
Scan type:	Fixed LOS (dual Doppler with Koshava)
Elevation angle (φ):	3.1 degrees
Elevation offset:	1.15 degrees
Azimuth angle (θ):	229.57 degrees
Azimuth offset:	2.82 degrees
Linear distance:	1613.74 m
Range gate to cup:	1625 m (41 range gates in total)
Position (UTM):	{448937.717, 6256404.894, 5.409}
Pulse length:	200 ns
Accumulation time:	500 ms
FFT size:	64

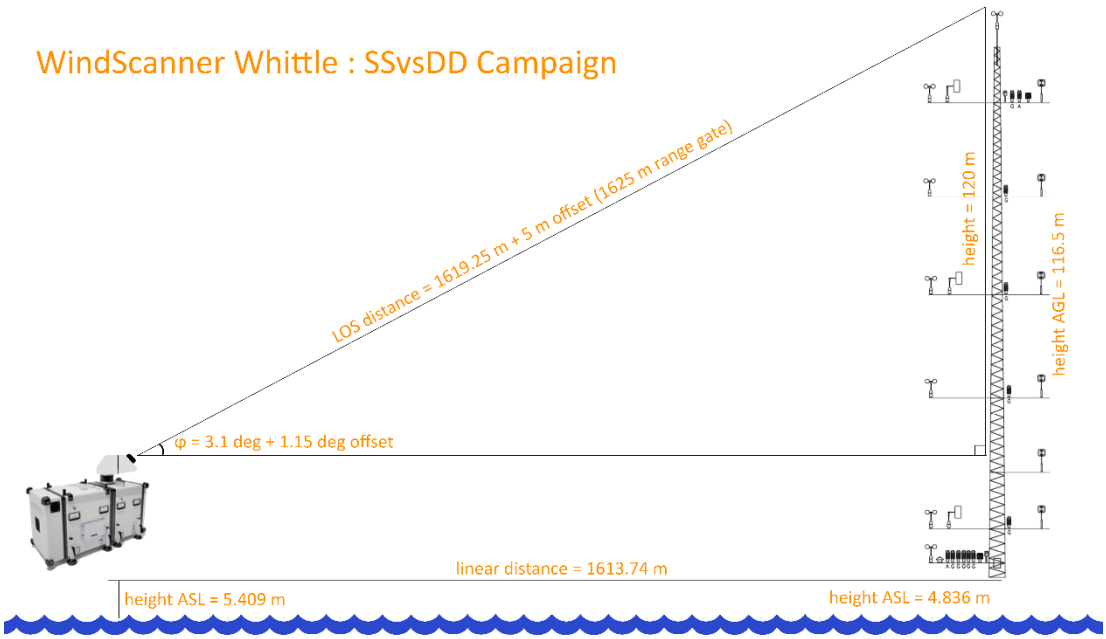

Figure 30: Whittle measurement geometry

5.6 Data

5.6.1 Structure / Overview

The WindScanner systems operate using complex monitoring, calculation and control processes. As such, a large amount of data is generated for numerous variables. Because the systems operate at different sampling rates, an asynchronous storage system has been implemented in order to prioritise certain variables (mainly motor control and scanner head positioning) over others such as device position (GPS coordinates, altitude) and movement (heading, pitch, roll). This conserves disk space, power draw and processing resources.

Each WindScanner records data locally within text based log files. The storage process is broken down into four parts: scenario, system, control and measurements. The variables and their interpretations are presented in the following section.

Raw data within the four tables is stored locally until retrieved via mobile 3/4G connection (SFTP) or manually copied via LAN, USB, etc. Next, they are loaded into DTU's internal MySQL server under a new schema created for each campaign.

Currently, there is no parallel processing of data into reconstructed wind speed and direction. Raw measurement data is post-processed according to the user's specifications. An automated data processing system will soon be developed at DTU, which outputs data on multiple levels depending on the user's needs.

5.6.2 WindScanner Database

The four database table structures are presented below. Variables and their significances are further detailed:

Table 7: Table overview of the WindScanner database

Scenario Table:		
scn_id (Scenario ID)	# (sequential)	(Primary key) Unique identifier within the campaign database assigned when new trajectory is loaded and executed. Disruption of measurement process also increments the scn_id field once resumed
scn_type (Scan Type)	LOS, PPI, RHI, DBS, CTC (complex continuous), CTD (complex discontinuous)	3 letter code indicating the type of scan being run. LOS = line of sight, PPI = plan position indicator, RHI = range height indicator, DBS = Doppler beam swinging, CTC or CTD = complex trajectory (such as virtual line or other pattern)
dt_start	seconds (decimal)	Timestamp at start of scan. Value is LabVIEW epoch (seconds after January 1, 1904
dt_stop	seconds (decimal)	Timestamp at end of scan. Same format as dt_start
gw_start_id	# (sequential)	First gw_id executed for each scn_id
gw_stop_id	# (sequential)	Last gw_id executed for each scn_id
pulse	ns	Pulse length (duration) of the laser. Value is set depending on targeted distance
fft (Fast Fourier Transform) size	# (64, 128, 256)	Resolution size of FFT function which converts the raw Doppler spectra (time domain) into frequency domain. Larger FFT size gives higher resolution, but takes longer to compute

System Table:		
Field	Unit / Value	Interpretation
scn_id (Scenario ID)	# (sequential)	Linked to scenario table (primary key)
dt	seconds (decimal)	Timestamp of measurement. Stamped at the end of the accumulation period. Same format as dt_start+stop
lati	decimal + N/S	Latitude in decimal form taken from GPS
longi	decimal + E/W	Longitude in decimal form taken from GPS
alti	m	Height above sea level (ASL)
head	degrees	Position angle relative to North
pitch	degrees	Tilt angle (forwards and backwards)
roll	degrees	Tilt angle (side to side)
temp	˚ C	Internal temperature of the WindScanner
humid	%	Relative humidity inside the WindScanner

Control Table:		
scn_id (Scenario ID)	# (sequential)	Linked to scenario table (primary key)
gw_id	# (sequential)	Global identifier for every scan executed within the scn_id
dt_start	seconds (decimal)	Linked to scenario table
dt_stop	seconds (decimal)	Linked to scenario table

azim	degrees	Azimuth position of scanner head for each measurement point. In dynamic scan types, the middle angle is recorded in the database
elev	degrees	Elevation position of scanner head for each measurement point. In dynamic scan types, the middle angle is recorded in the database
nbRG	#	Number of range gates recorded for the LOS (usually 41)
acc	ms	Accumulation time of photodetector after emitting the laser pulses. Longer accumulation time is needed for further distances, but will increase scanning time

Measurement Table:		
gw_id	# (sequential)	Global identifier for every scan executed within the scn_id
dist	decametre (10m)	LOS distance stamp for radSpeed and cnr. Measured in decametres (1dam = 10m)
radSpeed	m/s	Radial velocity measurement. Negative value represents aerosol moving away from WindScanner
cnr	dB	Carrier to noise ratio. Very high value represents interaction with hard target. Low value represents lack of signal. General expected range: -25 ≥ CNR (dB) ≤ 5
disp	#	Doppler (spectral) broadening due to non-uniform velocity distributions within the sampled volume

5.6.3 Met-Mast Instrumentation

The reference data used in this experiment comes from the 116.5m met-mast located at the south of the Høvsøre site. Internally this is referred to as the "tall mast" and is used often for commercial LiDAR calibrations. Each instrument's data logger has a different sampling rate, which is averaged into 10 minute periods and loaded into the DTU MySQL server. The mast contains the following instrumentation:

Table 8: Mast instrumentation at Høvsøre
Source: Source: (Peña et. al., 2015)

Measurement	Instrument	Height (m)
Wind speed	Risø P2546A cup anemometer	2, 10, 40, 60, 80, 100, and 116.5
Wind direction	Risø P2021A wind vane	10, 60, and 100
Relative Humidity	F2920A Vaisala HMP45A RH/ T probe radiation shield	2 and 100
Temperature Gradient	Risø P2642A sensor Risø P2029 radiation shield	2, 40, 60, 80, and 100 (relative to the lowest level–2)
Temperature (Absolute)	Risø P2449A sensor/ Risø P2029 radiation shield	−0.05, 2, and 100
Pressure	P2717A Vaisala barometer PTB100	2 and 100
Turbulence	Metek USA1 F2901A sonic	10, 20, 40, 60, 80, and 100
Solar radiation	F2253C CM11 pyranometer	2

A graphical summary of the instruments is also taken from (Peña et. al., 2015):

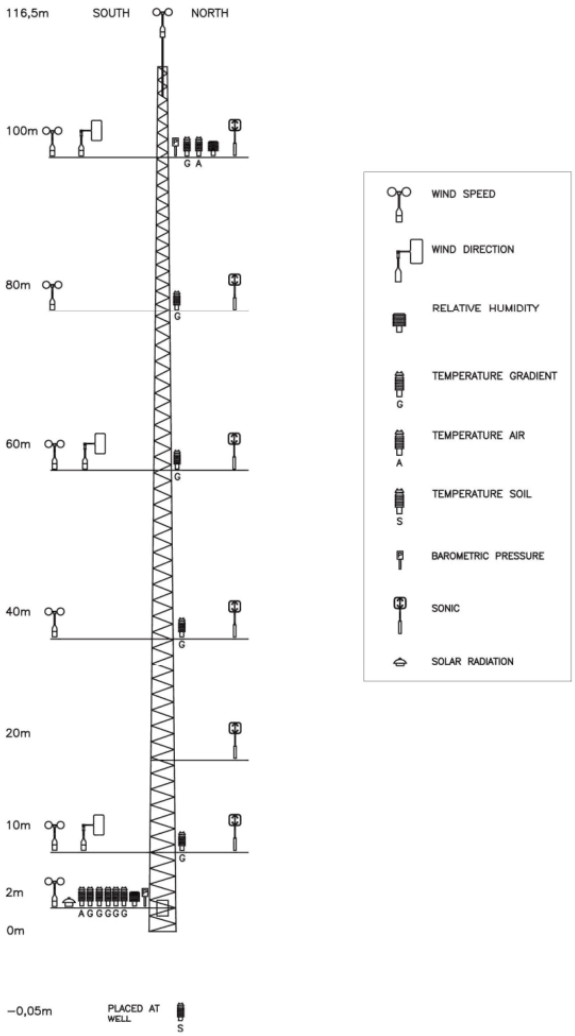

Figure 31: Overview of Høvsøre met-mast instrumentation
Source: (Peña et. al., 2015)

The calibration certificate for the 116.5m cup anemometer is attached in the appendix.

6 Results

6.1 Met-Mast / Reference

Using the data captured by the numerous instruments mounted on the met-mast, a detailed description of the site's atmospheric conditions can be made throughout the experiment. Summary statistics from the anemometer are shown in the following table:

Table 9: Summary statistics: Wind speed (cup anemometer) at 116.5m

Wind Speed (cup) at 116.5m	Value (m/s)
Minimum	1.799
1st quartile (middle value between minimum and median)	5.351
Median	7.783
Mean	7.840
3rd quartile (middle value between median and maximum)	10.292
Maximum	14.577

Along with a time series graph over the measurement period for wind speed:

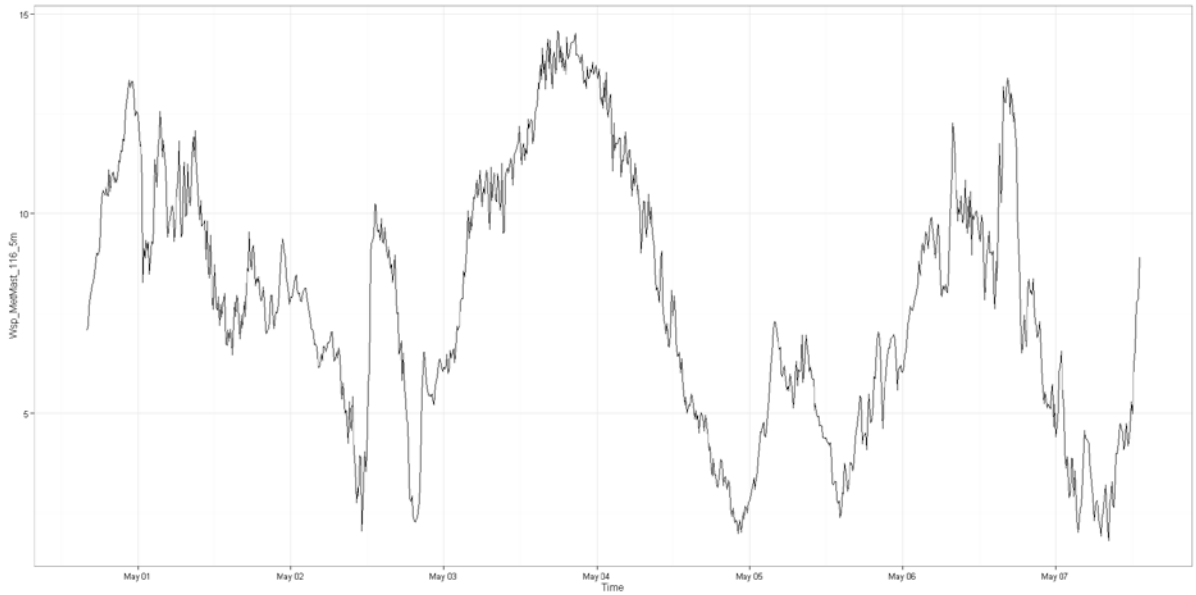

Figure 32: Time series: wind speed, met-mast cup anemometer at 116.5m

And wind direction:

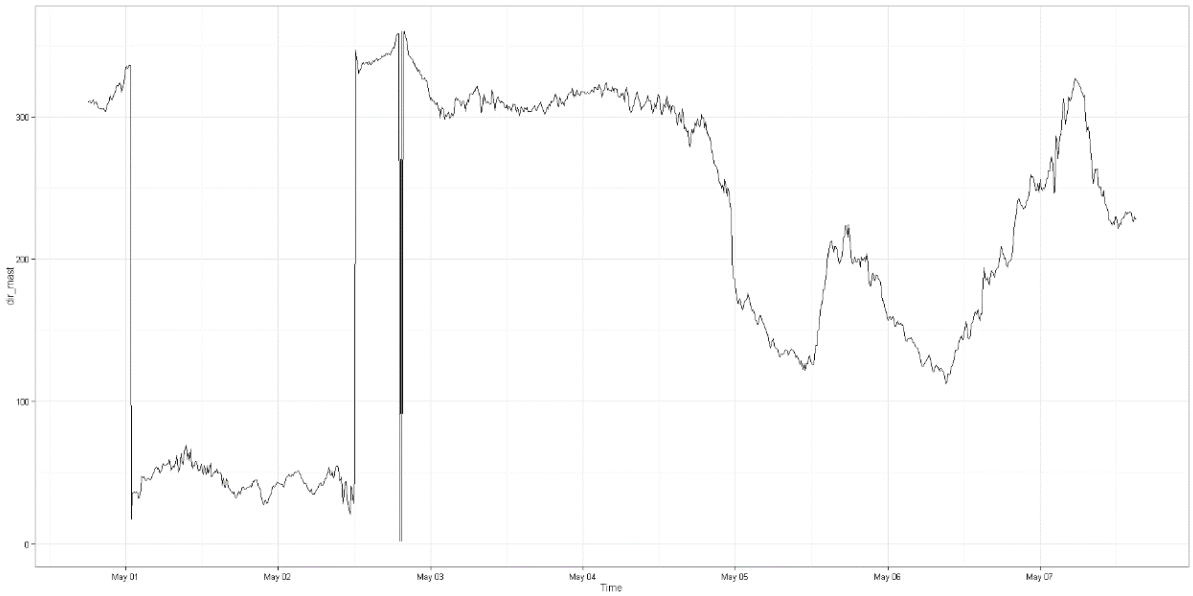

Figure 33: Time series: wind direction, met-mast vane at 100m

Leading to the following probability density functions, with rug plots indicating sample positions along the x axis:

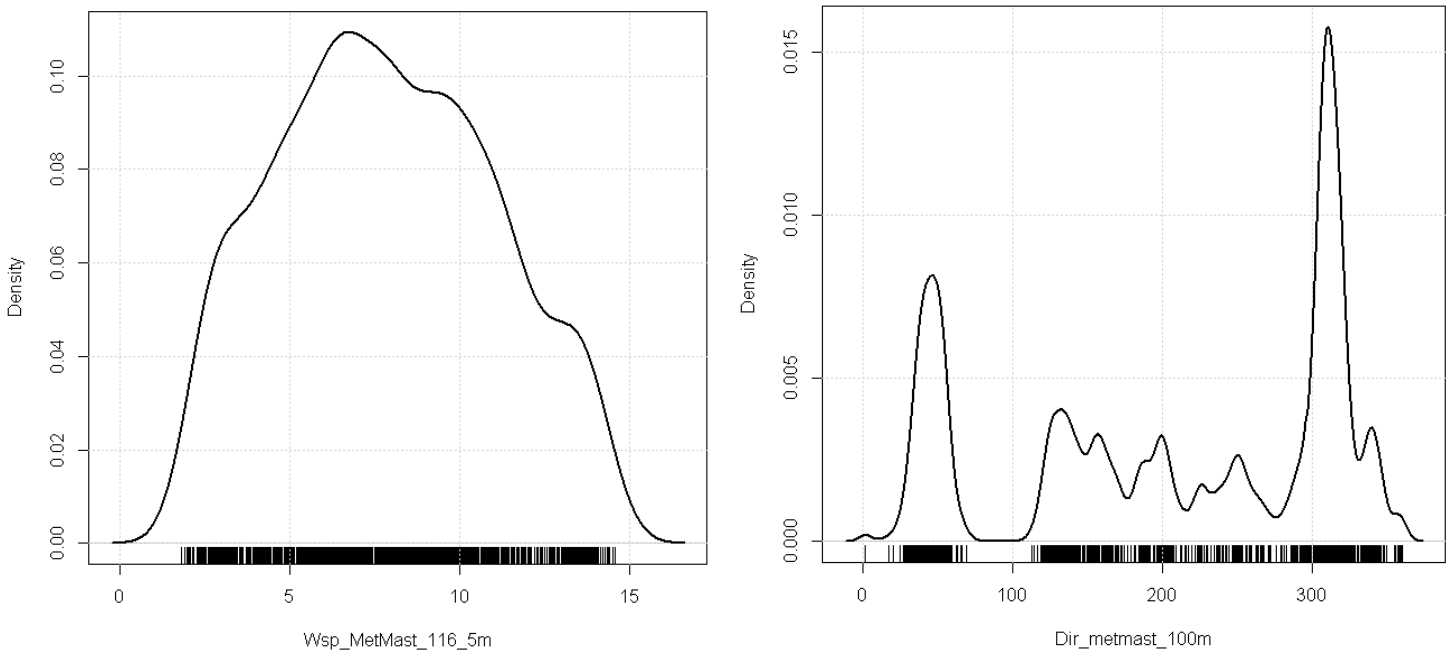

Figure 34: Probability density functions (PDF) of wind speed (116.5m) and direction (100m)

Through which we can fit a two-parameter Weibull function of scale (A = 8.9 m/s) and shape (k = 2.75) with a mean value of 7.9 m/s.

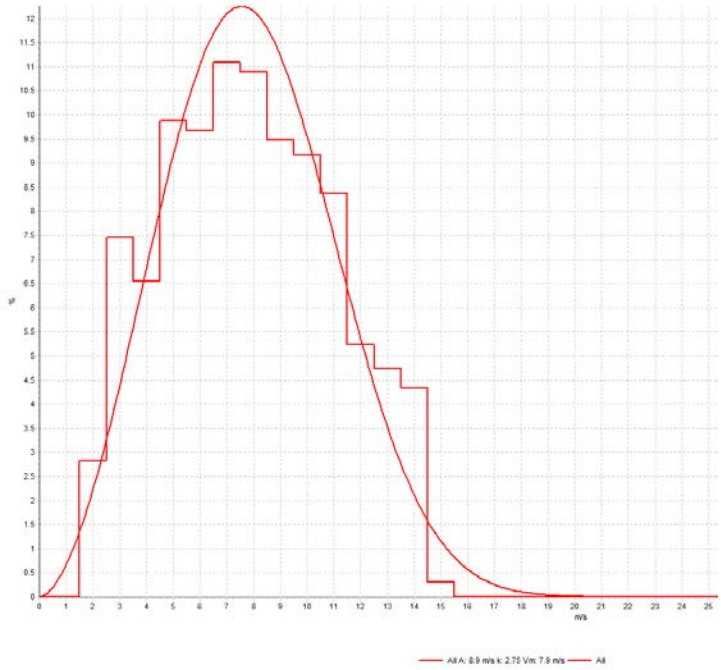

Figure 35: Weibull fit: wind speed at 116.5m

Further, we can inspect the variation in wind speeds over all instrumented heights (10, 40, 60, 80, 100 and 116.5m) through a time series graph:

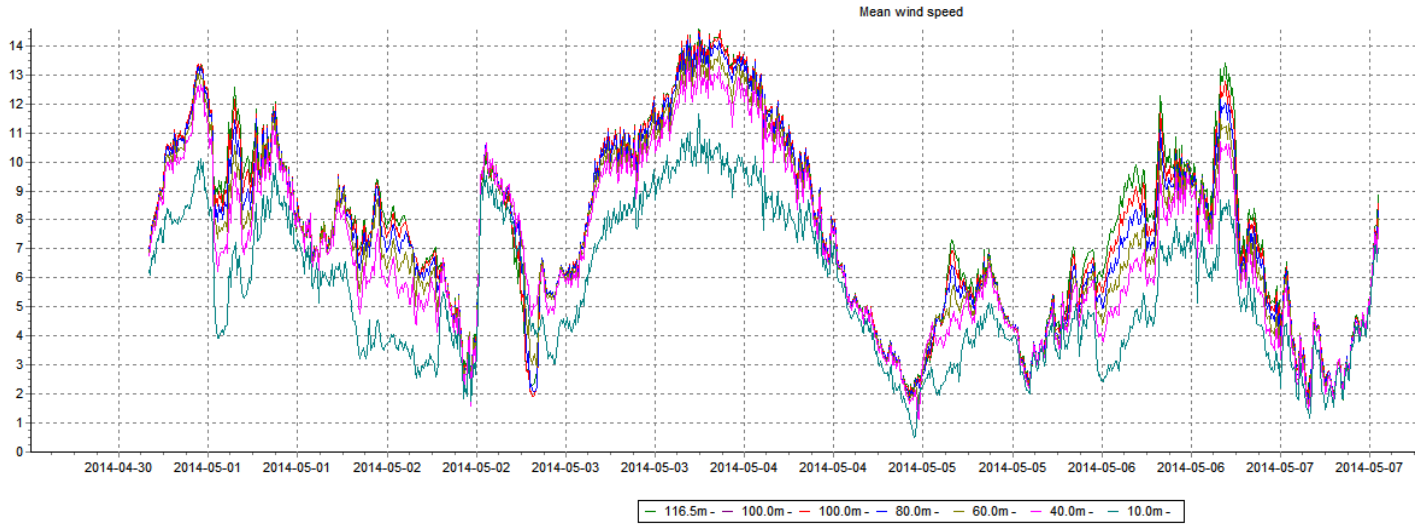

Figure 36: Time series: wind speed over heights 10, 40, 60, 80, 100 and 116.5m

And polar wind speed and direction roses over heights 10, 60, 100, and 116.5m:

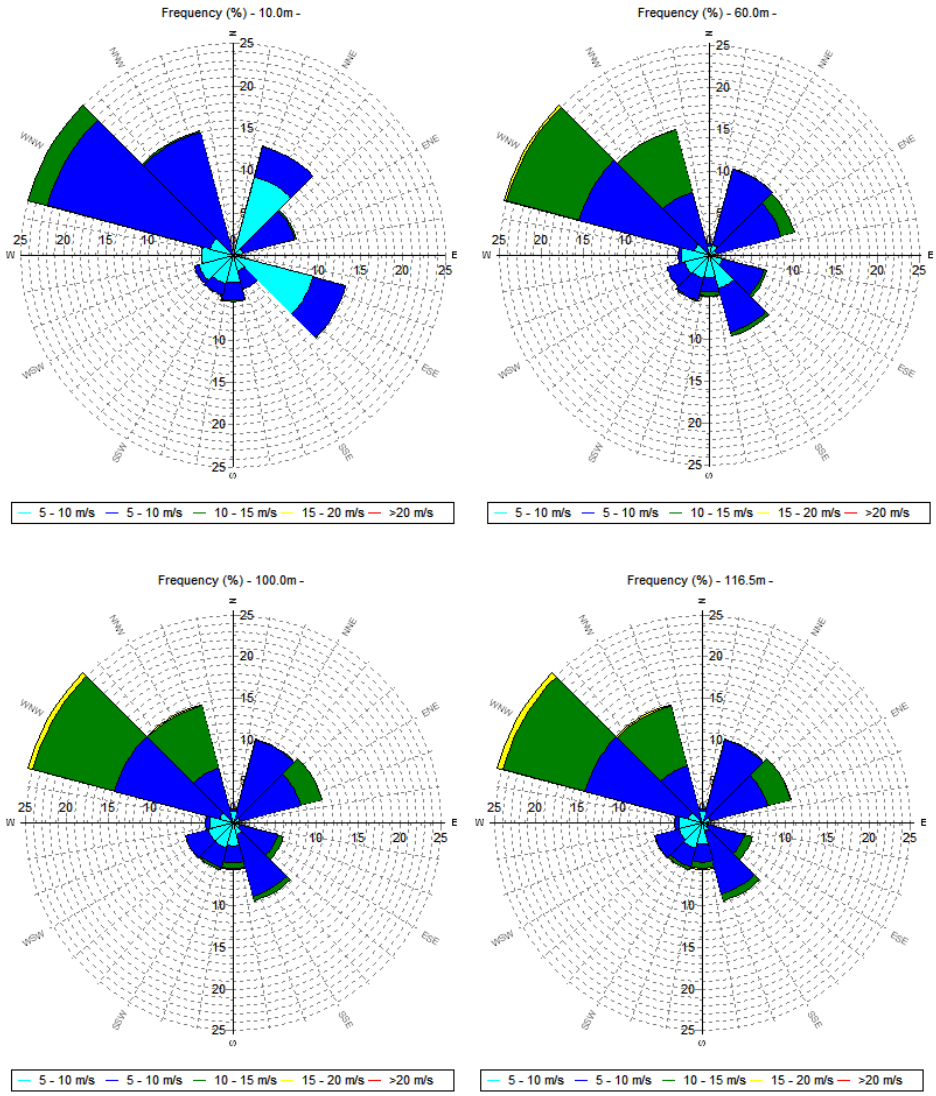

Figure 37: Wind roses over heights 10, 60, 100, 116.5m

Producing the following logarithmic wind profile:

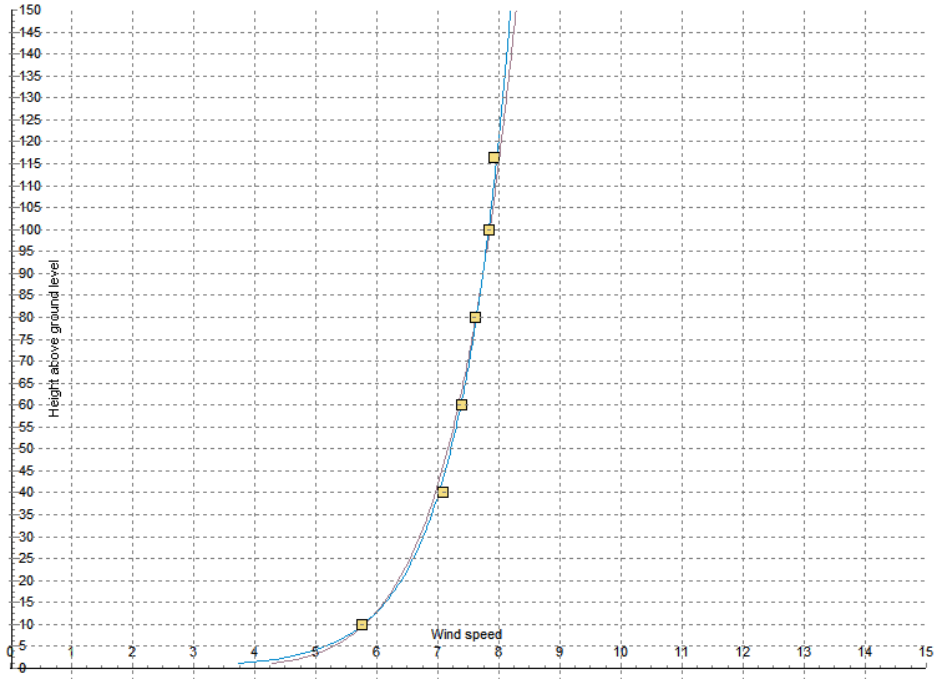

Figure 38: Vertical wind speed profile from 10-116.5m

From these results, we show that during the experiment period, site conditions are normal (vertical wind shear is within expectations) and that the reference instrumentation is operating correctly.

6.2 Dual Doppler

6.2.1 Time Series: Dual Doppler

The results from the dual Doppler analysis are presented in the following time series graphs for wind speed and direction. 10 minute averaged values are used.

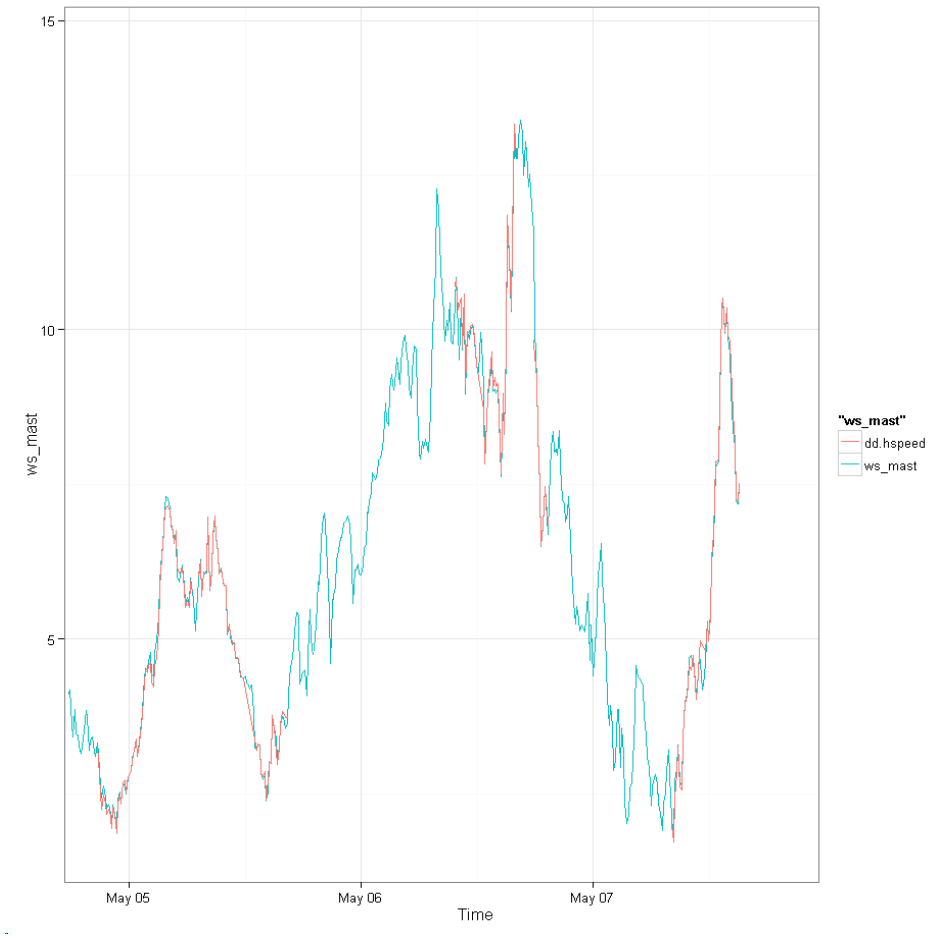

Figure 39: Time series graph: Dual Doppler vs. reference (wind speed)

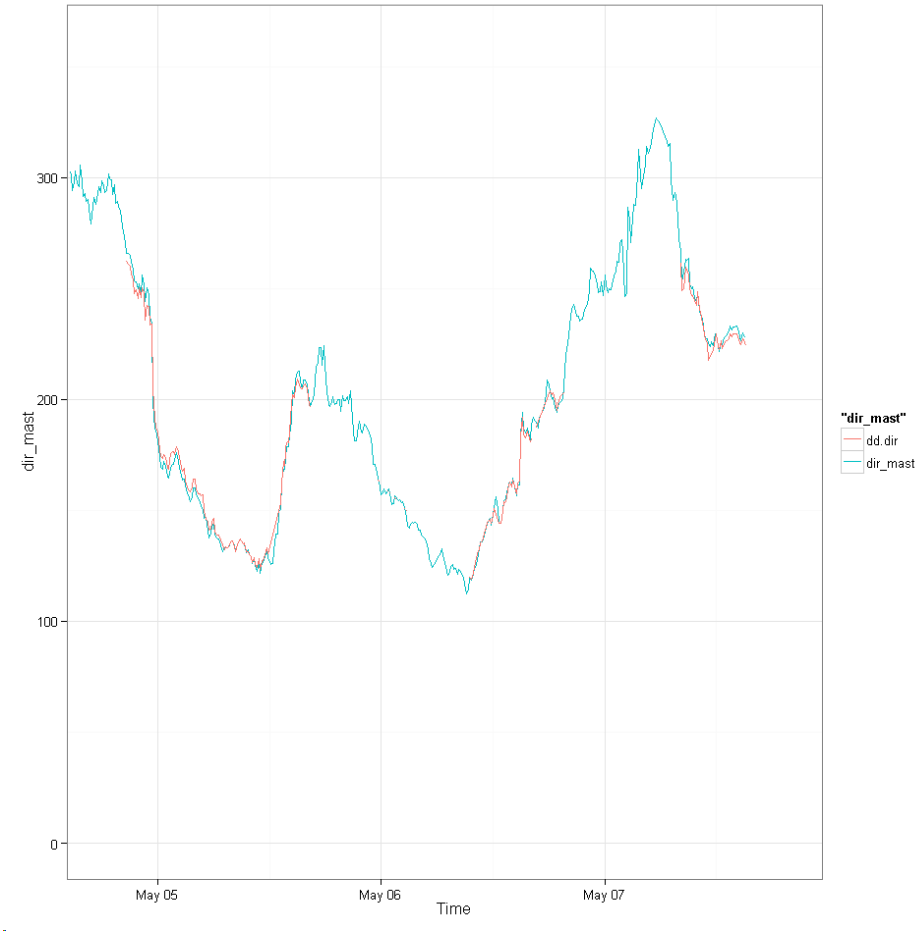

Figure 40: Time series graph: Dual Doppler vs. reference (wind direction)

6.2.2 Dual Doppler: Agreement with Reference

Scatterplots comparing the 10 minute averaged dual Doppler results to the reference (cup anemometer) are given in the following figures, along with the results of the linear fit models:

$$ws_{LiDAR} = ws_{mast} + 0 \text{ and } dir_{LiDAR} = dir_{mast} + \beta$$

6.2.3 Wind Speed

$$ws_{LiDAR} = (0.999)\, ws_{mast} + 0$$

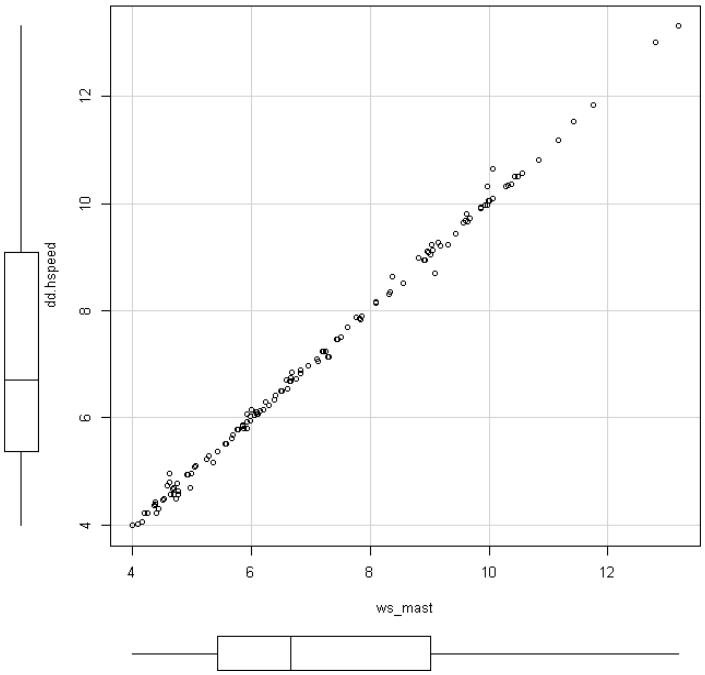

Figure 41: Scatterplot: Dual Doppler vs. reference (wind speed)

6.2.4 Wind Direction

$$dir_{LiDAR} = (1.024)\, dir_{mast} - 4.532$$

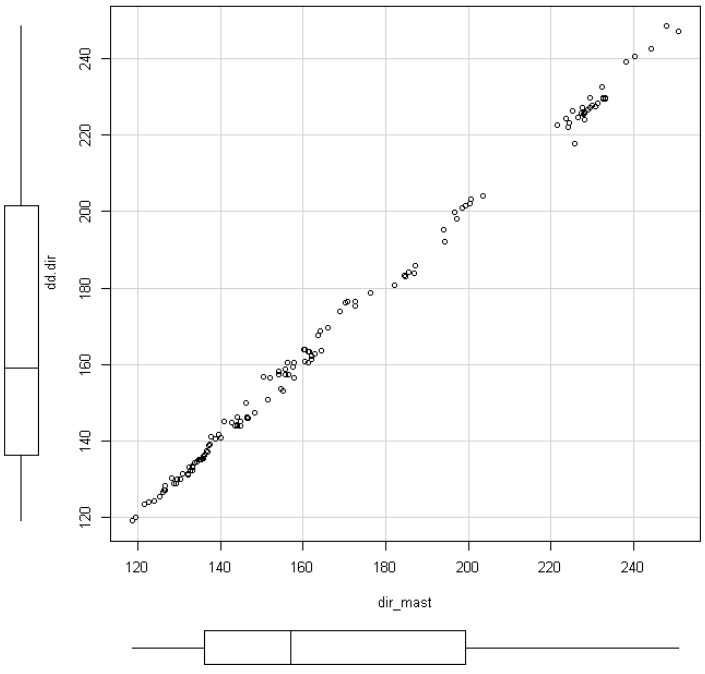

Figure 42: Scatterplot: Dual Doppler vs. reference (wind direction)

6.3 Sector Scan

6.3.1 Time Series: Sector Scan, 60 degrees

The results from the original (60 degree) sector scan analysis are presented in the following 10 minute averaged time series graphs for wind speed and direction.

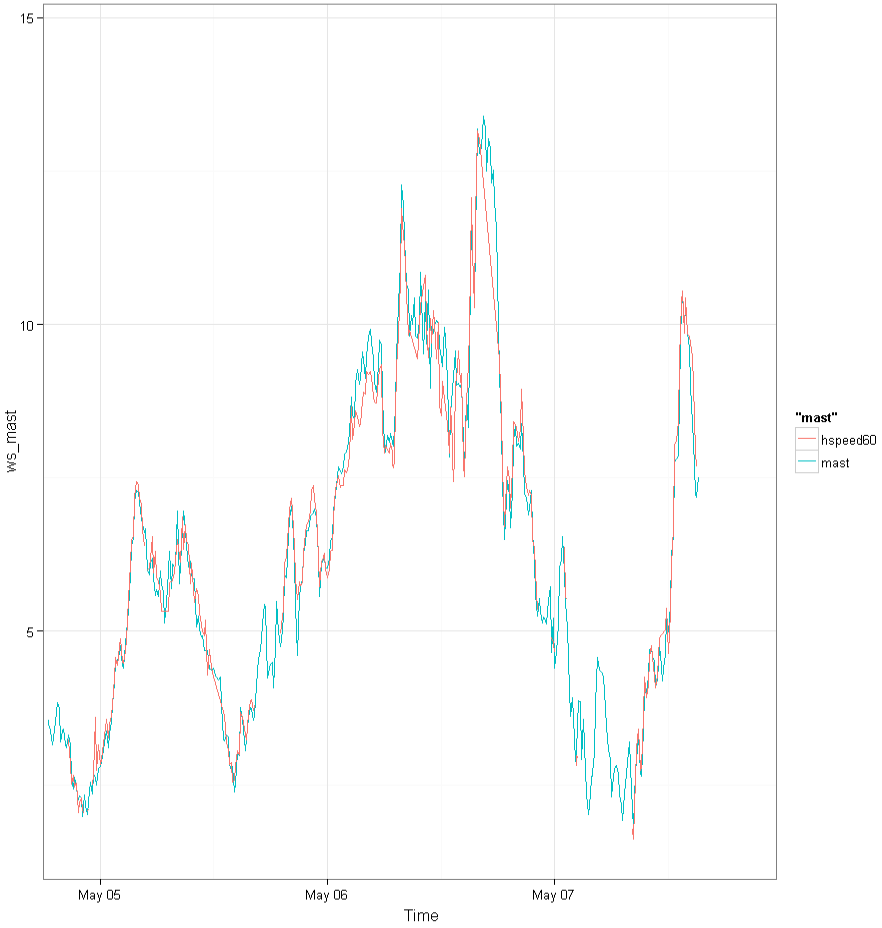

Figure 43: Time series, 60 degree sector scan vs. cup (wind speed)

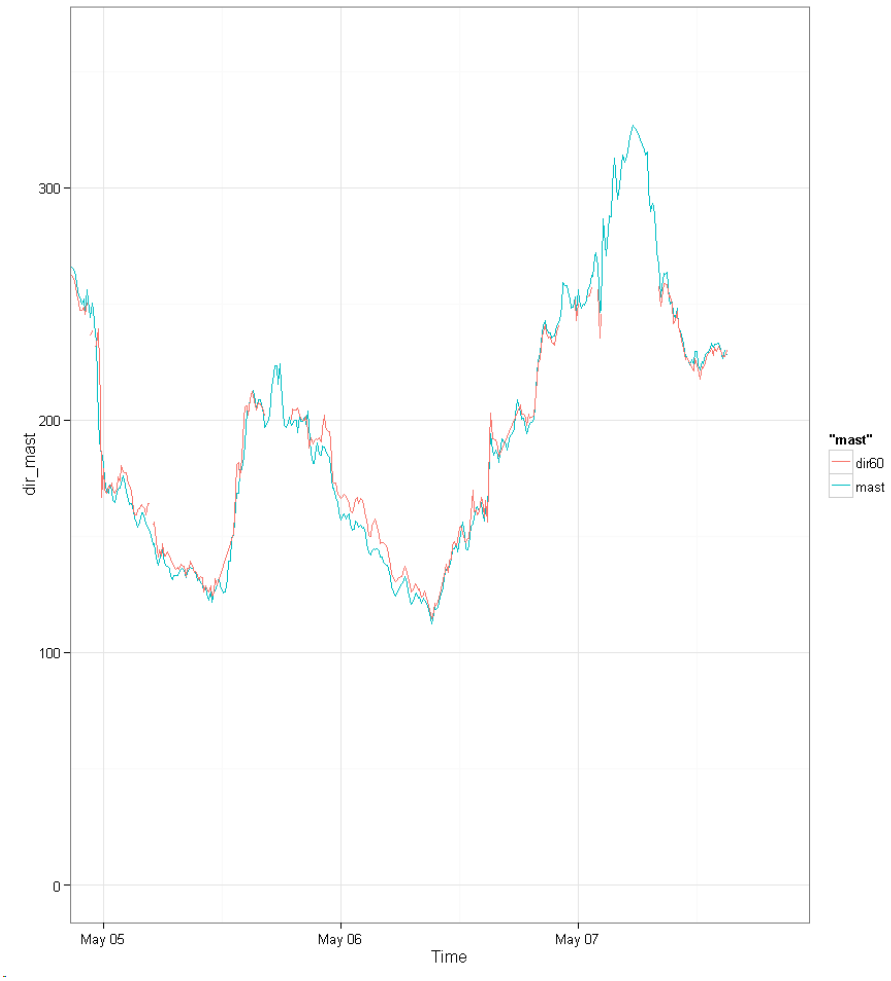

Figure 44: Time series, 60 degree sector scan vs. cup (wind direction)

6.3.2 Plot Matrix: Sector Size Variations

The SSvsDD dataset has been reconstructed using opening angles: 60, 50, 44, 38, 30, 22, 14, 8 and 4 degrees. The purpose of which is to determine the effect of larger and smaller sector sizes on the: overall shape (linear regression coefficient), overall fit (r^2 coefficient), amount of scatter (residuals) and bias of scatter (under/over prediction).

The plots comparing the reconstructed 10 minute averaged wind speed and direction from the LiDAR to the collocated cup anemometer (reference measurement) are given in the following section. Boxplots are also included along both the x and y axes, which represent (starting from the origin) the minimum, first quartile (middle value between minimum and median), median, third quartile (middle value between median and maximum), and maximum values. An investigation of the scatterplot, linear fit model and the boxplot will together indicate the how well the reconstructed data matches the reference instrumentation.

For readers using electronic mediums, animated versions of the wind speed and direction results are presented in:

Appendix C: Animated Results, which exhibits the degradation of the fitted results as the sector size decreases.

6.3.3 Wind Speed

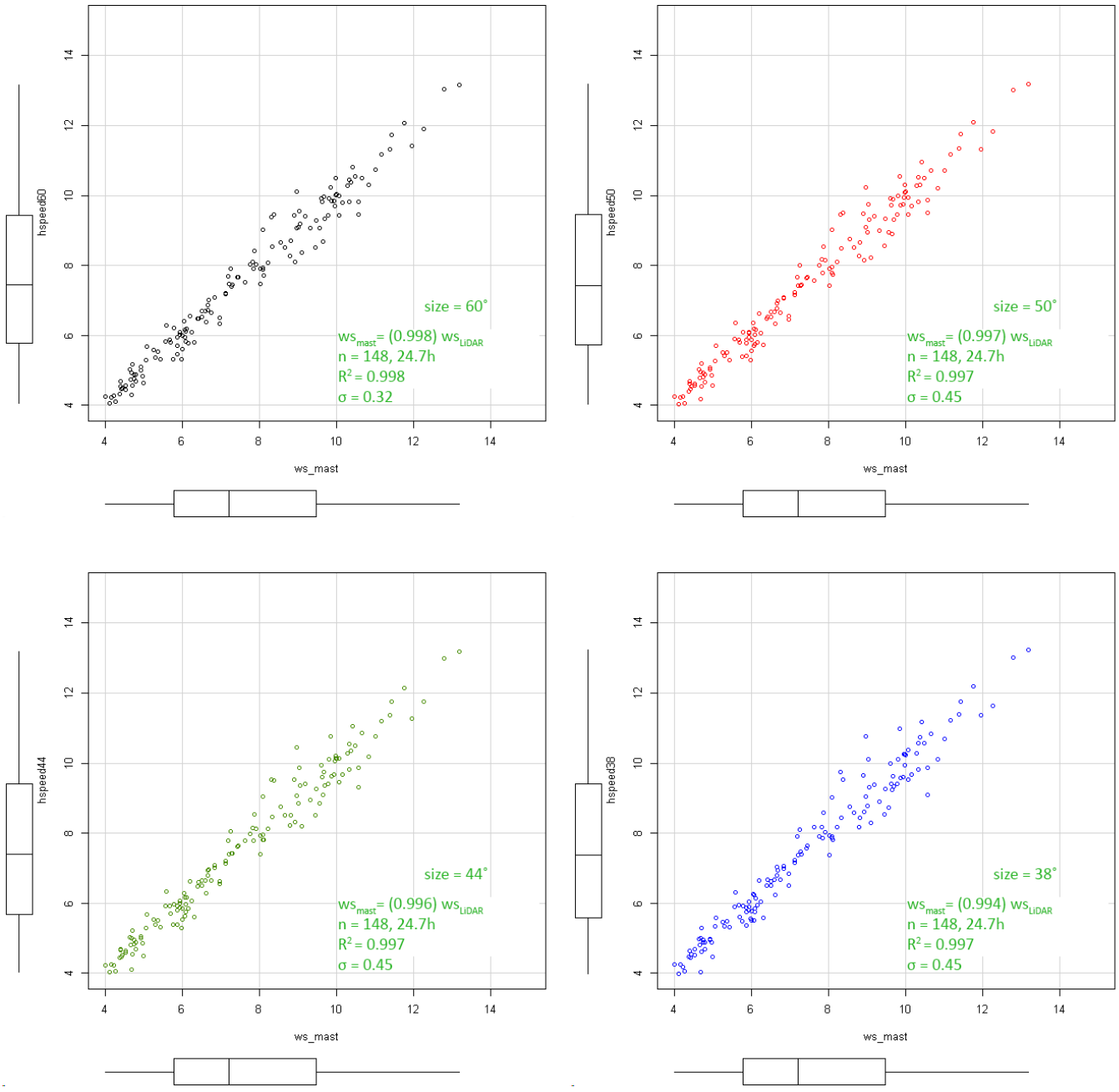

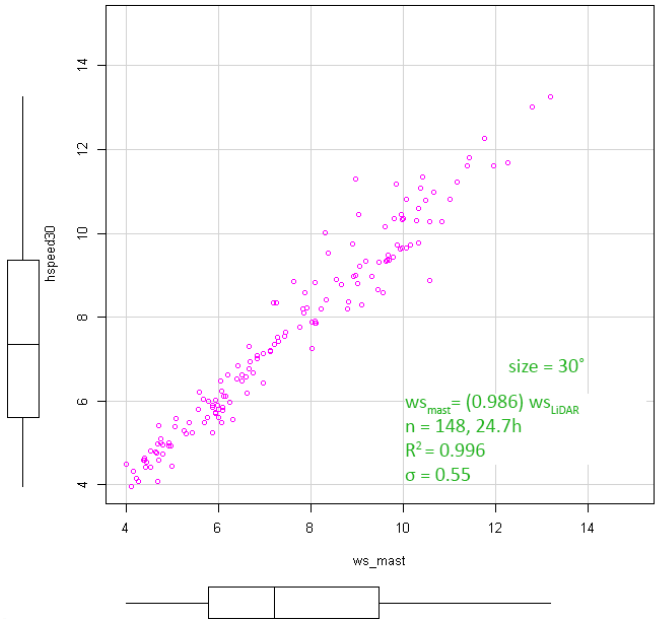
hspeed30
ws_mast
size = 30°
ws_mast= (0.986) ws_LiDAR
n = 148, 24.7h
R² = 0.996
σ = 0.55

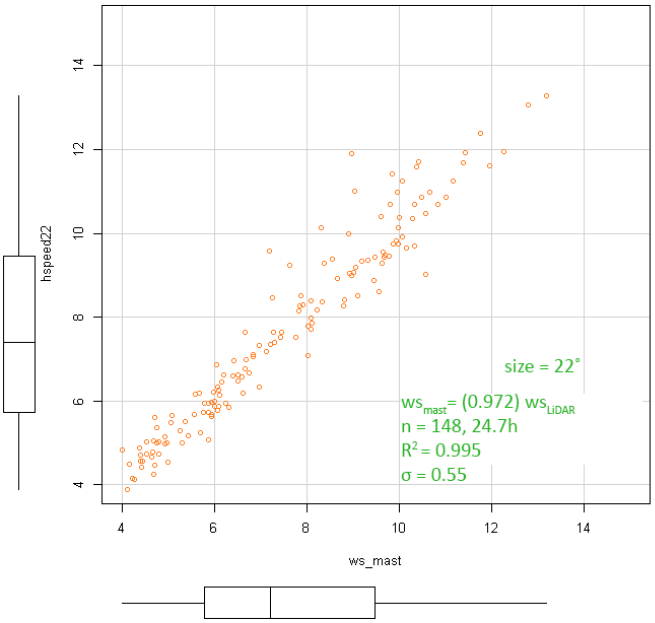
hspeed22
ws_mast
size = 22°
ws_mast= (0.972) ws_LiDAR
n = 148, 24.7h
R² = 0.995
σ = 0.55

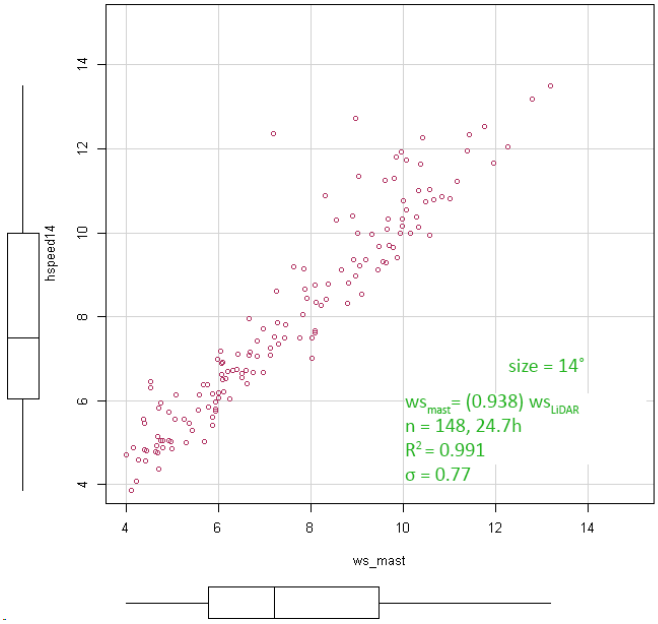
hspeed14
ws_mast
size = 14°
ws_mast= (0.938) ws_LiDAR
n = 148, 24.7h
R² = 0.991
σ = 0.77

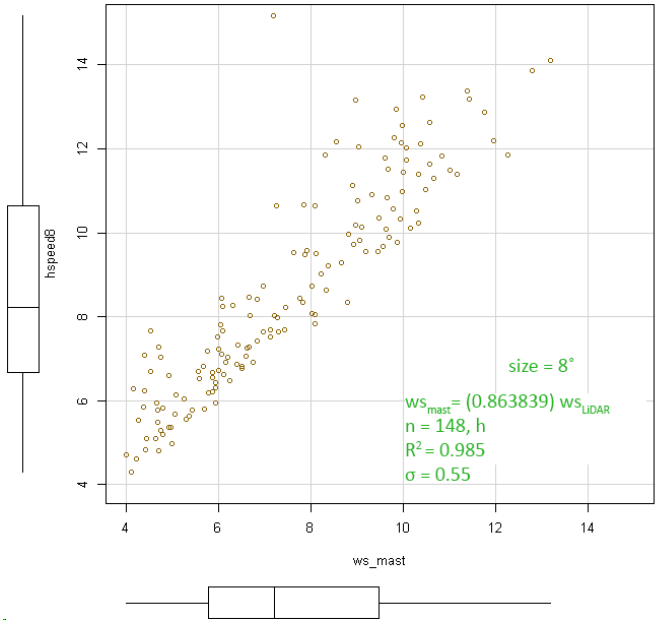
hspeed8
ws_mast
size = 8°
ws_mast= (0.863839) ws_LiDAR
n = 148, h
R² = 0.985
σ = 0.55

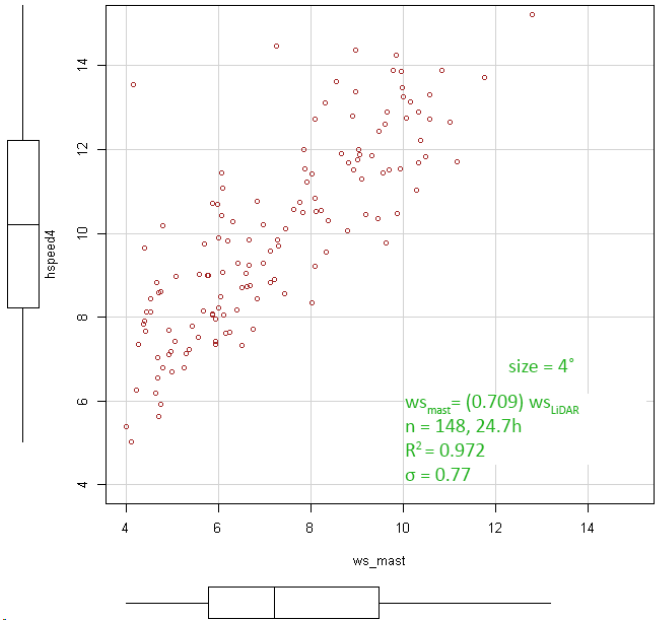

Figure 45: Scatterplots of various sector sizes vs. reference wind speed (SSvsDD)

6.3.4 Wind Direction

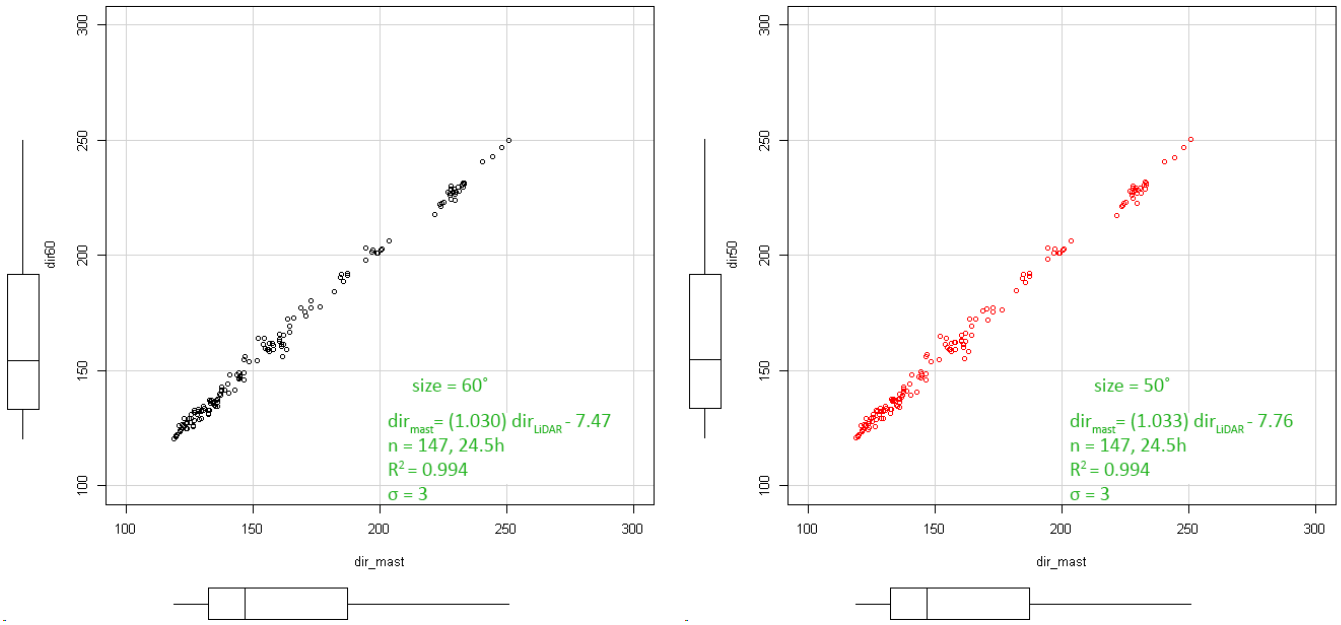

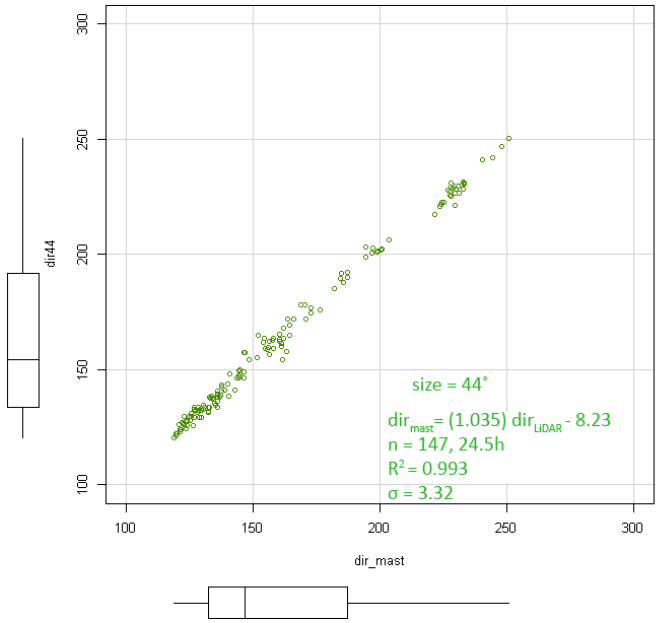
dir44
dir_mast
size = 44°
dir_mast = (1.035) dir_LiDAR - 8.23
n = 147, 24.5h
R² = 0.993
σ = 3.32

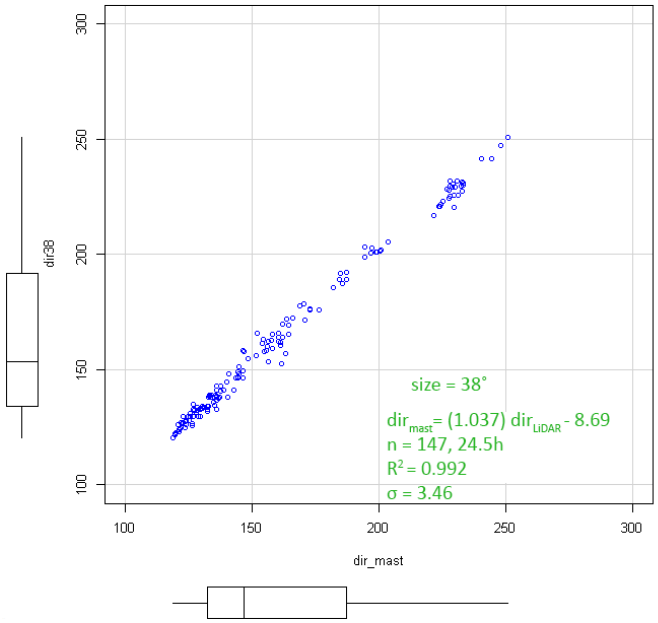
dir38
dir_mast
size = 38°
dir_mast = (1.037) dir_LiDAR - 8.69
n = 147, 24.5h
R² = 0.992
σ = 3.46

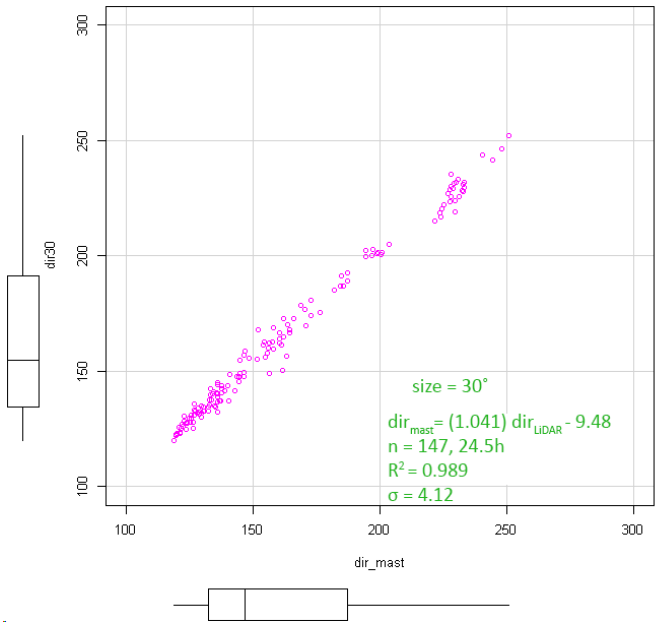
dir30
dir_mast
size = 30°
dir_mast = (1.041) dir_LiDAR - 9.48
n = 147, 24.5h
R² = 0.989
σ = 4.12

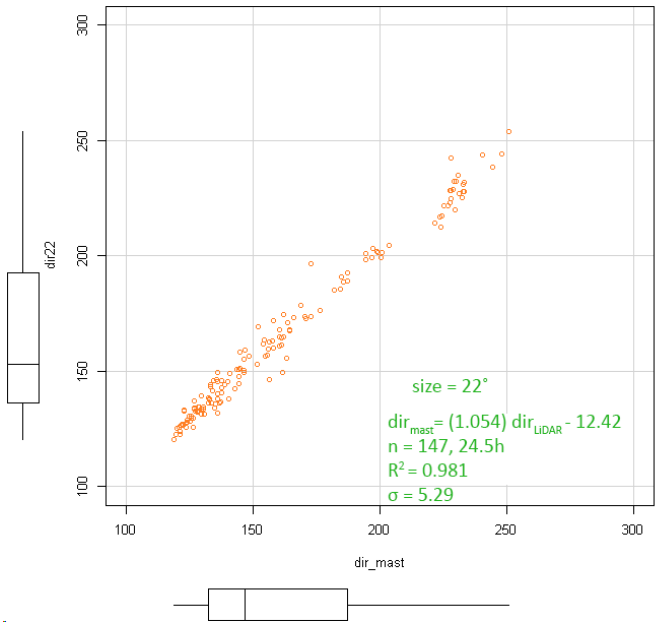
dir22
dir_mast
size = 22°
dir_mast = (1.054) dir_LiDAR - 12.42
n = 147, 24.5h
R² = 0.981
σ = 5.29

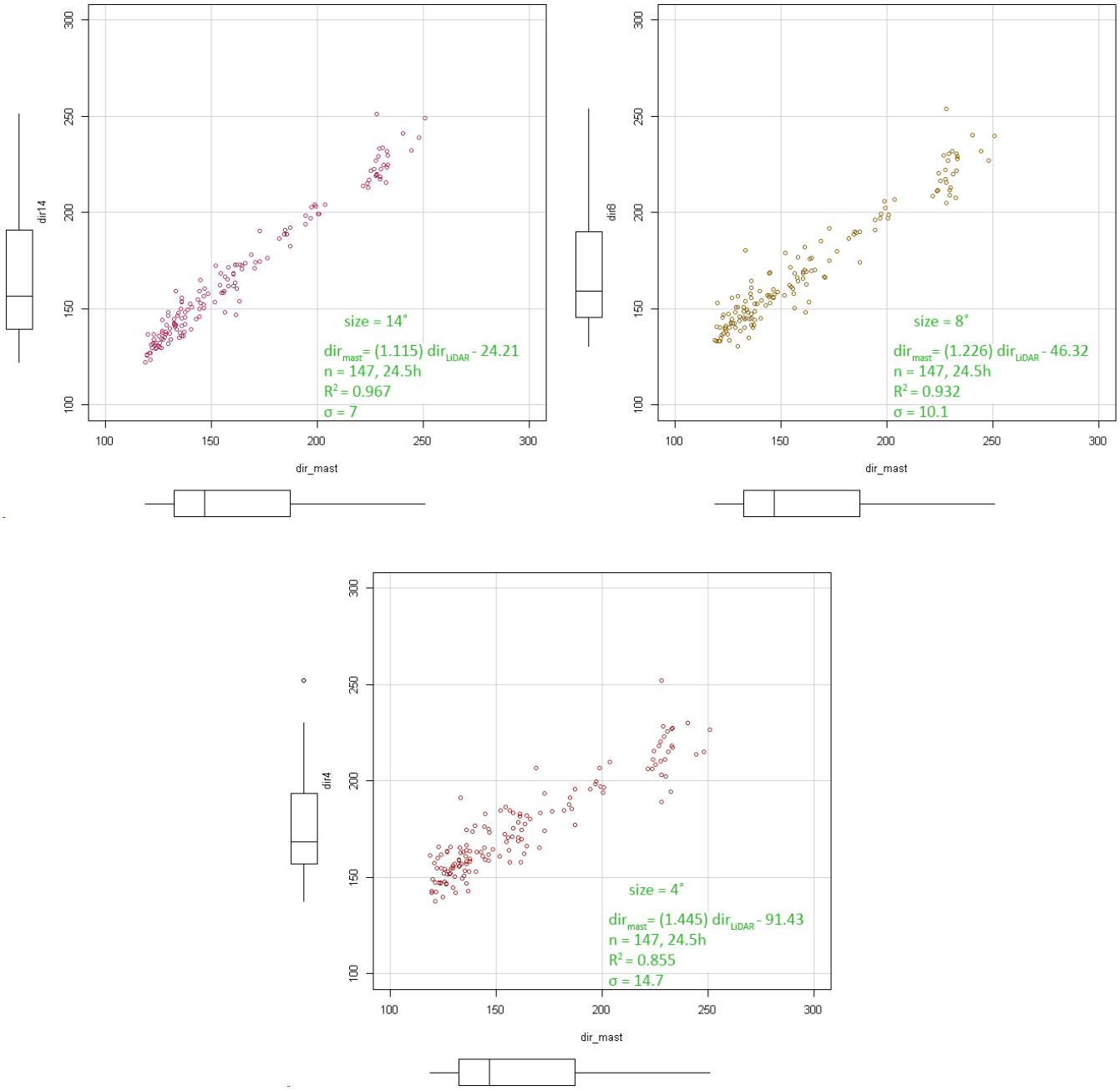

Figure 46: Scatterplots of various sector sizes vs. reference wind direction (SSvsDD)

6.3.5 Table of Statistics

The following tables list the most important statistical parameters of the linear fit models:

$$ws_{mast} = \alpha\, ws_{LiDAR} + 0 \text{ and } dir_{mast} = \alpha\, dir_{LiDAR} + \beta$$

Table 10: Result of linear fit models (reconstructed wind speed vs. reference) of various sector size reconstructions (SSvsDD)

sector size (degrees)	number of samples	coefficient	r^2	median residual	standard deviation of residuals (σ)
60	148	0.998046	0.9977	-0.05815	0.32
50	148	0.997089	0.9975	-0.05689	0.45
44	148	0.996350	0.9972	-0.05475	0.45
38	148	0.994067	0.9968	-0.02647	0.45
30	148	0.985658	0.9959	0.01645	0.55
22	148	0.972177	0.9945	0.1011	0.55
14	148	0.93811	0.9907	0.1650	0.77
8	148	0.863839	0.9851	0.2135	0.55
4	148	0.709620	0.9719	0.2182	0.77

Table 11: Result of linear fit models (reconstructed wind direction vs. reference) of various sector size reconstructions (SSvsDD)

sector size (degrees)	n	coefficient	intercept (β)	r^2	median residual	standard deviation of residuals (σ)
60	147	1.030948	-7.469123	0.9941	0.2452	3
50	147	1.032669	-7.761162	0.9937	0.1382	3
44	147	1.034897	-8.225787	0.9929	0.0286	3.32
38	147	1.037025	-8.686731	0.9918	-0.0286	3.46
30	147	1.040643	-9.481138	0.9888	0.0106	4.12
22	147	1.05417	-12.41524	0.981	0.338	5.29
14	147	1.1147	-24.2111	0.9671	0.1242	7
8	147	1.22598	-46.32213	0.9315	0.204	10.1
4	147	1.44477	-91.42641	0.8546	0.157	14.7

7 Discussion & Conclusion

7.1 Sector Scan vs. Dual Doppler Comparison

Results from the dual Doppler and sector scan analyses both show excellent agreement overall with the mast instrumentation. Linear fit coefficient estimates for wind speed of 0.999 (dual Doppler) and 0.998 (60˚ sector scan) along with high r^2 values show that on average, wind speeds are accurately measured using both techniques. Similar results are obtained for wind direction.

When examining wind speed measurement performance, the sector scan approach exhibits larger amounts of scatter (higher residuals) on a systematic level. The bias of scatter (over/under prediction) appears to be uniformly distributed. The wind speed range between 8-11 m/s also exhibits larger errors in this particular case.

The sector scan results perform just as well as dual Doppler for wind direction retrieval. The author's hypothesis for this is that wind direction tends to be more homogeneous in undisturbed flow than wind speeds. This means that the assumption of horizontal homogeneity contributes a smaller error than the case for wind speed reconstruction.

In conclusion, for project developers simply interested in performing a site level resource analysis, with the goal of obtaining broadly accurate 10 minute averaged wind speed and direction values, the sector scan method is appropriate and recommended. The addition of a second scanning LiDAR in dual Doppler mode would be an extraneous investment, which would not considerably improve the accuracy of the result. For other purposes in which a minimised error is essential, then the dual Doppler configuration is shown to perform better for the case of retrieved wind speeds.

7.2 Optimum sector size

From comparing linear fit models for the various sector size reconstructions against the reference instrumentation, it is shown that there is no significant difference between using a wide scanning angle of 60˚ compared to 30˚. To further demonstrate this point, time series graphs are presented which compare the mast with 30 and 60 degree reconstructions:

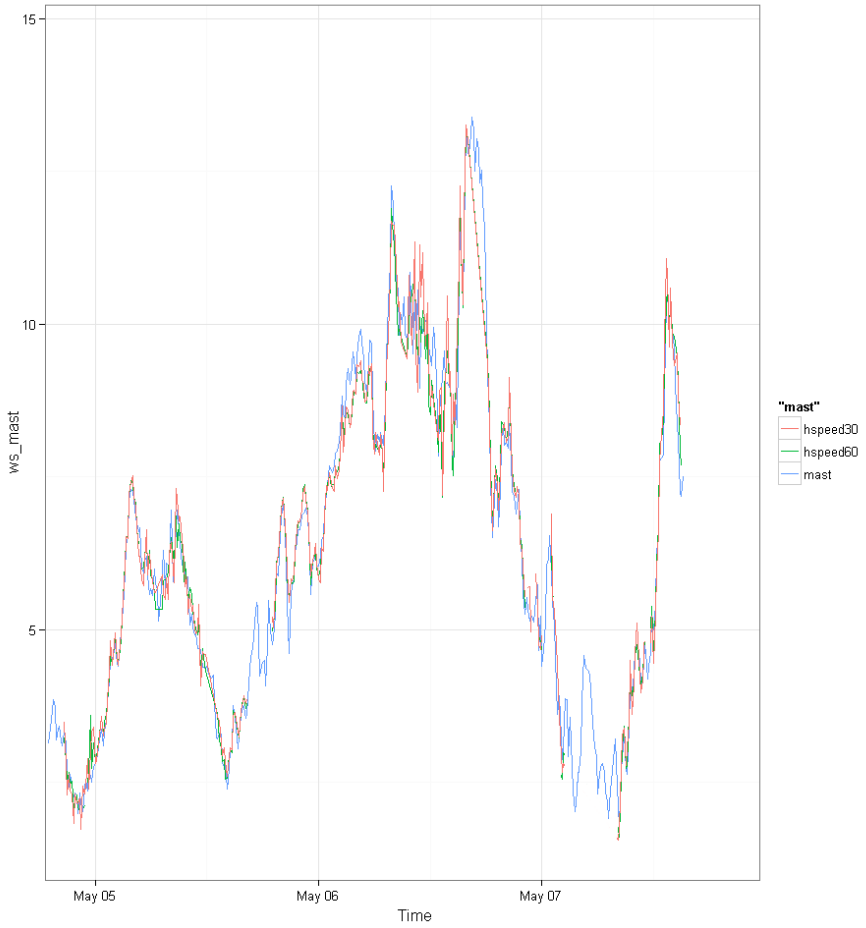

Figure 47: Time series comparison: mast vs. 60 vs. 30 degree sector scan (wind speed)

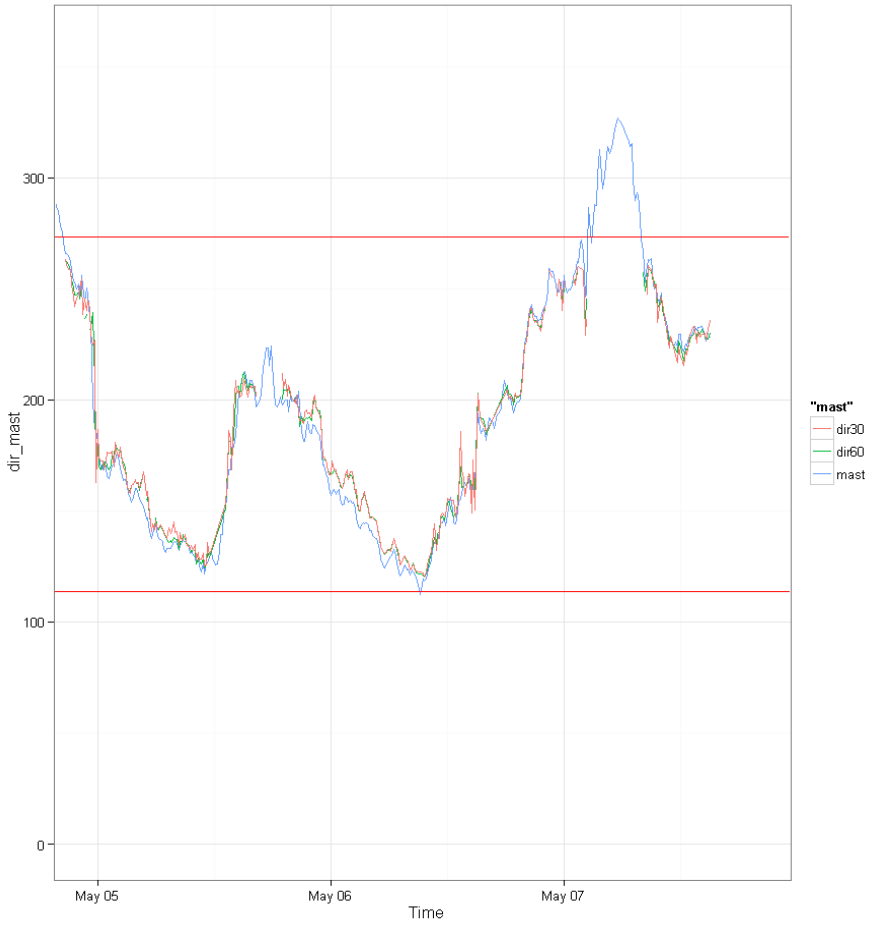

Figure 48: Time series comparison: mast vs. 60 vs. 30 degree sector scan (wind direction)

It appears the optimum case lies between 30 and 38 degrees. Using angles smaller than 30 degrees quickly degrades the relationship for both wind speed and direction.

It is postulated that this result is due to the larger atmospheric volume being sampled with increased sector sizes, and the assumption of homogeneity within the volume. Taking an area larger than necessary to derive the vector components will not improve the quality of the result.

This is a significant outcome, which will be further verified in the RUNE campaign. Using a smaller sector size has numerous advantages over larger areas when systematic error is unaffected. Utilising a 30 degree sector size compared to 60 degrees leads to twice the sampling rate of the system (which reduces averaging error). Further it opens the possibility to dedicate the saved time to increasing the pulse backscatter acquisition length (leading to further measurement distances), and/or to increase the scan's resolution by lowering the angular azimuth separation. Additionally, it allows for more precise targeting of the area of interest, particularly at large distances.

8 Proposed Extension of Work

Although outside the scope of this thesis project, some ideas on how to continue the work of understanding and optimising sector scan usage are presented here. Many of these topics will be incorporated into future experiments, such as RUNE.

- Automated filtering
  It should be possible to automate the CNR and radial speed filtering steps with some basic signal processing techniques, either during the acquisition period or by post-processing the CNR and radial speed values. One hypothesized approach is to examine the shape of the signal over a moving average and determine high resolution filters which can adjust dynamically to the stable conditions. This implementation would lead to an increase in available data points as well as reduce time spent on data cleaning. In order to preserve (potentially desirable) artifacts including turbulence and for device troubleshooting, it is suggested that for non-commercial purposes this automation take place after the data has been acquired normally (through post-processing).

- Reducing measurement uncertainty
  As mentioned earlier, factors such as the dynamic scanner head positioning, LiDAR support platform rigidity, experimental design, etc. all contribute to the overall quality of the measurements. Investigation and improvement along this theme is currently being undertaken by the WindScanner development team, in particular Nikola Vasiljević.

- Higher elevation angles
  It may be necessary in some scenarios to measure at higher elevation angles. Due to the limitations imposed by the SDVR approach, it is not possible to determine the vertical component of the wind flow using a single LiDAR. Thus, it is unknown whether the results of this study would apply to higher elevation angles. The forthcoming experimental hub height "balconies" at the Østerild test center will allow for further research in this area.

- Goodness of fit parameter
  There were plans to include this feature in the AAS, but they were never fully realised. It would be useful to create a reference value which could be used in the filtering stage, which represents how well the points fit to the sine wave. In some cases, a single or series of abnormal points can cause the fitting function to be shifted or misaligned. The ability to filter out these deviances with an additional variable would be immensely helpful.

References

Barratt, P., Browne, I.C., 1953. A new method for measuring vertical air currents. Q.J.R. Meteorol. Soc. 79, 550–550. doi:10.1002/qj.49707934218

Bent, A.E., Massachusetts Institute of Technology, Radiation Laboratory, 1943. Radar echoes from atmospheric phenomena. Radiation Laboratory, Massachusetts Institute of Technology, [Cambridge, Mass.].

Boybeyi, Z., 2015. Wind Vector Components [WWW Document]. George Mason University. URL http://wx.gmu.edu/dev/clim301/lectures/wind/wind-uv.html (accessed 8.3.15).

Browning, K.A., Wexler, R., 1968. The Determination of Kinematic Properties of a Wind Field Using Doppler Radar. J. Appl. Meteor. 7, 105–113. doi:10.1175/1520-0450(1968)007<0105:TDOKPO>2.0.CO;2

Brown, R.A., Peace Jr, R.L., 1968. Mesoanalysis of convective storms utilizing observations from two Doppler radars, in: Preprints, 13th Radar Meteor. Conf., Montreal, QC, Canada, Amer. Meteor. Soc. pp. 188–191.

Cariou, J.-P., Augere, B., Valla, M., 2006. Laser source requirements for coherent lidars based on fiber technology. Comptes Rendus Physique, High power fiber lasers and amplifiersLasers et amplificateurs à fibre de puissance 7, 213–223. doi:10.1016/j.crhy.2006.03.012

Cariou, J.-P., Sauvage, L., Thobois, L., Gorju, G., Machta, M., Lea, G., Duboué, M., 2011. Long range scanning pulsed Coherent Lidar for real time wind monitoring in the Planetary Boundary Layer. 16th CLRC.

Courtney, M., Wagner, R., Murthy, R.K., Boquet, M., 2014. Optimized lidar scanning patterns for reduced project uncertainty.

Creative Commons, 2015. Creative Commons — Attribution-ShareAlike 4.0 International — CC BY-SA 4.0 [WWW Document]. URL https://creativecommons.org/licenses/by-sa/4.0/legalcode (accessed 9.21.15).

DTU Wind Energy, 2015. Test Centre for large wind turbines at Høvsøre [WWW Document]. http://www.vindenergi.dtu.dk. URL http://www.vindenergi.dtu.dk/English/About/Hoevsoere_uk.aspx (accessed 9.9.15).

Henderson, S., 2013. Review of Fundamental Characteristics of Coherent and Direct Detection Doppler Receivers and Implications to Wind Lidar System Design.

Lhemitte, R., Atlas, D., 1961. Precipitation motion by pulse Doppler, in: Proc. Ninth Weather Radar Conf., Boston, Amer. Meteor. Soc. pp. 218–223.

Lhermitte, R.M., 1970. Dual-Doppler radar observations of convective storm circulation, in: 14th Conference on Radar Meteorology (preprints). pp. 139–144.

Meinberg GmbH, 2015. Time Synchronization in Electrical Systems [WWW Document]. URL https://www.meinbergglobal.com/english/info/time-synchronization-electrical-systems.htm#start (accessed 8.4.15).

Mie, G., 1908. Beiträge zur Optik trüber Medien, speziell kolloidaler Metallösungen. Annalen der physik 330, 377–445.

Newsom, R.K., Berg, L.K., Shaw, W.J., Fischer, M.L., 2015. Turbine-scale wind field measurements using dual-Doppler lidar. Wind Energ. 18, 219–235. doi:10.1002/we.1691

Paschotta, R., 2015a. Encyclopedia of Laser Physics and Technology - coherence, coherent, light, spatial and temporal coherence, monochromaticity [WWW Document]. URL https://www.rp-photonics.com/coherence.html (accessed 9.9.15).

Paschotta, R., 2015b. Encyclopedia of Laser Physics and Technology - optical heterodyne detection, balanced detection, homodyne detection, coherent detection [WWW Document]. URL https://www.rp-photonics.com/optical_heterodyne_detection.html (accessed 9.15.15).

Peña, A., Floors, R., Sathe, A., Gryning, S.-E., 1, R.W., Courtney, M.S., Larsén, X.G., Hahmann, A.N., Hasager, C.B., 2015. Ten Years of Boundary-Layer and Wind-Power Meteorology at Høvsøre, Denmark. doi:10.1007/s10546-015-0079-8

Premasundaran, M., 2015. Properties of Lasers [WWW Document]. URL http://www.worldoflasers.com/laserproperties.htm (accessed 9.9.15).

Sathe, A., Mann, J., Vasiljevic, N., Lea, G., 2015. A six-beam method to measure turbulence statistics using ground-based wind lidars. Atmospheric Measurement Techniques 8, 729–740. doi:10.5194/amt-8-729-2015

Schwiesow, R.L., Köpp, P., Werner, C., 1985. Comparison of CW-Lidar-Measured Wind Values Obtained by Full Conical Scan, Conical Sector Scan and Two-Point Techniques. J. Atmos. Oceanic Technol. 2, 3–14. doi:10.1175/1520-0426(1985)002<0003:COCLMW>2.0.CO;2

SgurrEnergy, Clive, P., 2014. Why, when and how to use Lidar : SgurrEnergy Webinar [WWW Document]. URL http://www.sgurrenergy.com/about-sgurr-energy/download-centre/webinars/ (accessed 9.22.15).

Siemens Wind Power, 2015. Siemens - SWT-2-3-93 [WWW Document]. URL http://www.energy.siemens.com/us/en/renewable-energy/wind-power/platforms/g2-platform/wind-turbine-swt-2-3-93.htm (accessed 8.25.15).

Vasiljević, N., 2014a. A time-space synchronization of coherent Doppler scanning lidars for 3D measurements of wind fields, DTU Wind Energy PhD. DTU Wind Energy.

Vasiljević, N., 2014b. Windscanner.eu Laser show at Rödeserberg [WWW Document]. URL http://www.windscanner.eu/index.php/component/content/article/15-news-frontend/51-laser-show-at-roedeserberg (accessed 9.16.15).

Vasiljević, N., 2014c. WindScanner systems - IRPWind. EERA IRPWind & Joint Programme Wind R&D Conference 2014, 2014, Amsterdam.

Vasiljević, N., Lea, G., Courtney, M., Mann, J., Mikkelsen, T., 2013a. The long-range WindScanner system – how to synchronously intersect multiple laser beams. European Wind Energy Association (EWEA).

Vasiljević, N., Lea, G., Courtney, M., Schneemann, J., Trabucchi, D., Trujillo, J.-J., Unguran, R., Villa, J.-P., 2013b. The application layer protocol: Remote Sensing Communication Protocol (RSComPro). DTU Wind Energy.

Venter, A.D., Vakkari, V., Beukes, J.P., Zyl, V., G, P., Laakso, H., Mabaso, D., Tiitta, P., Josipovic, M., Kulmala, M., Pienaar, J.J., Laakso, L., 2012. An air quality assessment in the industrialised western Bushveld Igneous Complex, South Africa. South African Journal of Science 108, 1–10.

Windl, U., 2003. How do Computer Clocks work? [WWW Document]. URL http://www.eecis.udel.edu/~ntp/ntpfaq/NTP-s-sw-clocks.htm (accessed 8.4.15).

Appendix A: AAS Source Code

The AAS source code is released open source under the Creative Commons Attribution-ShareAlike 4.0 International License. The licensing terms are available at (Creative Commons, 2015.

Sector scan AAS:
http://elliot-simon.com/msc-thesis/sectorscan.py
Mirror: https://github.com/elliotsimon/msc-thesis/blob/master/sectorscan.py

Dual Doppler AAS:
http://elliot-simon.com/msc-thesis/dualdoppler.py
Mirror: https://github.com/elliotsimon/msc-thesis/blob/master/dualdoppler.py

Appendix B: Raw Data

Sector scan CNR & radial speed graphs:
http://elliot-simon.com/msc-thesis/ss-data.pdf
Mirror: https://github.com/elliotsimon/msc-thesis/blob/master/ss-data.pdf

Dual Doppler Sector scan CNR & radial speed graphs:
http://elliot-simon.com/msc-thesis/dd-data.pdf
Mirror: https://github.com/elliotsimon/msc-thesis/blob/master/dd-data.pdf

Appendix C: Animated Results

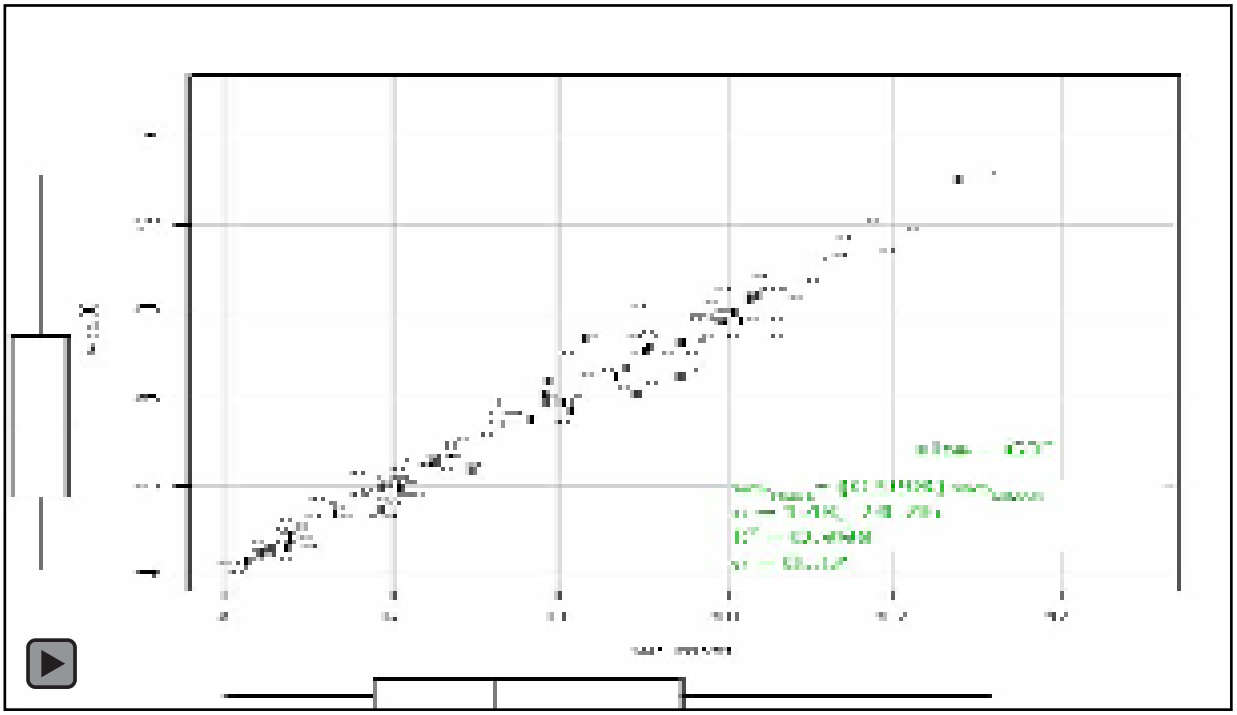

Figure 49: Animated result: Wind speed sector size

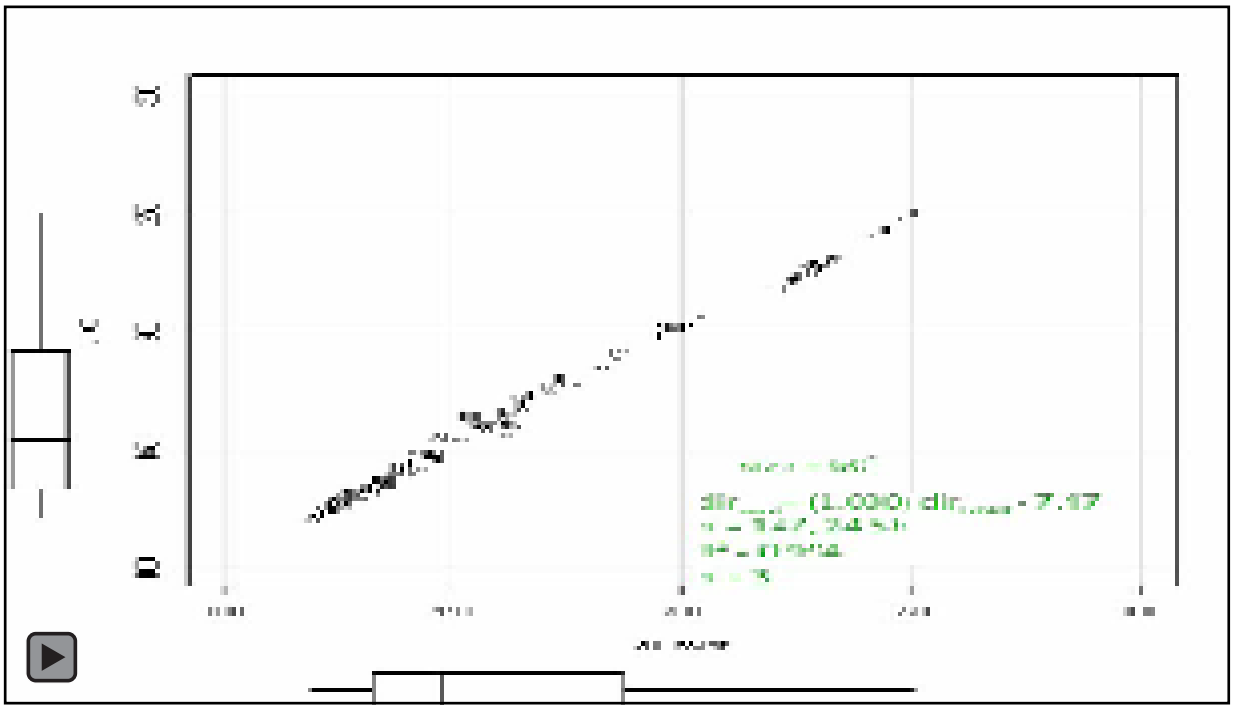

Figure 50: Animated result: Wind direction sector size

Appendix D: WindPRO Meteo Data Export

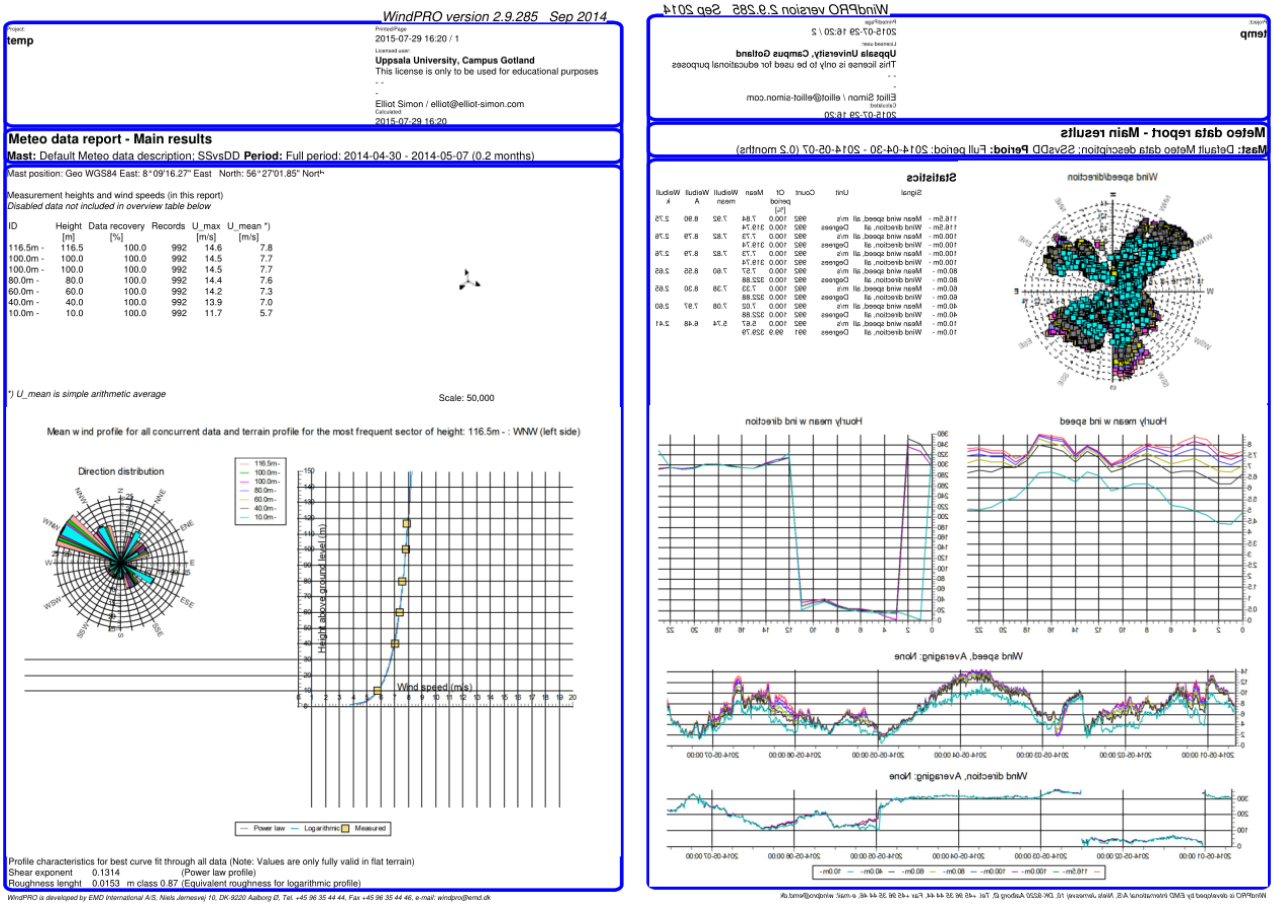

WindPRO version 2.9.285 Sep 2014

temp

2015-07-29 16:20 / 1

Uppsala University, Campus Gotland

This license is only to be used for educational purposes

Elliot Simon / elliot@elliot-simon.com

2015-07-29 16:20

Meteo data report - Main results

Mast: Default Meteo data description; SSvsDD **Period:** Full period: 2014-04-30 - 2014-05-07 (0.2 months)

Mast position: Geo WGS84 East: 8°09'16.27" East North: 56°27'01.85" North

Measurement heights and wind speeds (in this report)

Disabled data not included in overview table below

ID	Height [m]	Data recovery [%]	Records	U_max [m/s]	U_mean *) [m/s]
116.5m -	116.5	100.0	992	14.6	7.8
100.0m -	100.0	100.0	992	14.5	7.7
100.0m -	100.0	100.0	992	14.5	7.7
80.0m -	80.0	100.0	992	14.4	7.6
60.0m -	60.0	100.0	992	14.2	7.3
40.0m -	40.0	100.0	992	13.9	7.0
10.0m -	10.0	100.0	992	11.7	5.7

*) U_mean is simple arithmetic average

Scale: 50,000

Mean w ind profile for all concurrent data and terrain profile for the most frequent sector of height: 116.5m - : WNW (left side)

Direction distribution

Height above ground level (m)

Wind speed (m/s)

Power law Logarithmic Measured

Profile characteristics for best curve fit through all data (Note: Values are only fully valid in flat terrain)

Shear exponent 0.1314 (Power law profile)

Roughness lenght 0.0153 m class 0.87 (Equivalent roughness for logarithmic profile)

WindPRO is developed by EMD International A/S, Niels Jernesvej 10, DK-9220 Aalborg Ø, Tel. +45 96 35 44 44, Fax +45 96 35 44 46, e-mail: windpro@emd.dk

Statistics

Hourly mean w ind direction

Hourly mean w ind speed

Wind speed, Averaging: None

Wind direction, Averaging: None

Appendix E: Cup Anemometer Calibration Results

Kalibrierschein
Calibration certificate

Gegenstand *Object*	Cup Anemometer
Hersteller *Manufacturer*	WindSensor DK-4000 Roskilde
Typ *Type*	P2546A-OPR
Fabrikat/Serien-Nr. *Serial number*	5543 3140
Auftraggeber *Customer*	Risoe DTU DK-4000 Roskilde
Auftragsnummer *Order No.*	VT140675
Anzahl der Seiten des Kalibrierscheines *Number of pages of the certificate*	3
Datum der Kalibrierung *Date of calibration*	26.06.2014

Kalibrierergebnis:
Result:

File:	1413414	
Test Item	Tunnel Speed	Uncertainty (k=2)
Hz	m/s	m/s
6.271	4.085	0.050
9.469	6.038	0.055
12.451	7.882	0.050
15.450	9.720	0.051
18.587	11.663	0.057
21.707	13.624	0.051
24.928	15.576	0.057
23.253	14.550	0.051
20.212	12.657	0.053
17.043	10.693	0.056
13.865	8.781	0.051
10.805	6.879	0.056
7.930	5.137	0.050

Appendix F: Extraction of Dual Doppler from Unsynchronised PPI Scans

F.1 Abstract

The wisscas experimental setup includes two WindScanners which are operating in 45 degree PPI (sector scan) mode. Because the WindScanners have been calibrated such that the centre of their scanning arcs intersect at a single point in space (directly above the met-mast), it is in theory possible to extract dual Doppler estimations from the dataset.

However, the experiment was not designed with this analysis in mind and thus the WindScanners were not programmed to sync their scanning trajectories in both space and time.

For this dataset, requiring both lines of sight to be measured at the same point (above the met-mast) at the same exact time by both WindScanners yielded zero values. An accepted gap in time between when both beams cross the measurement point was then added into the SQL query. A brief study was done in order to determine the effect of different time gaps on: the number of samples, the fit of a linear regression vs. 10 minute averaged met-mast data, and the shape and amount of scatter around the regression line. The SQL query within the Dual Doppler Automated Analysis Software (DD AAS) was adjusted to accept time gaps of: 0.5, 2, 5 and 8 seconds between both WindScanners measuring at the given position. The result graphs from this study are presented below. Although all cases resulted in very good agreement, due to the high number of samples, reduction of scatter and closer fit to the regression line, a time gap of 5 seconds is determined to be optimal.

F.2 Result Graphs

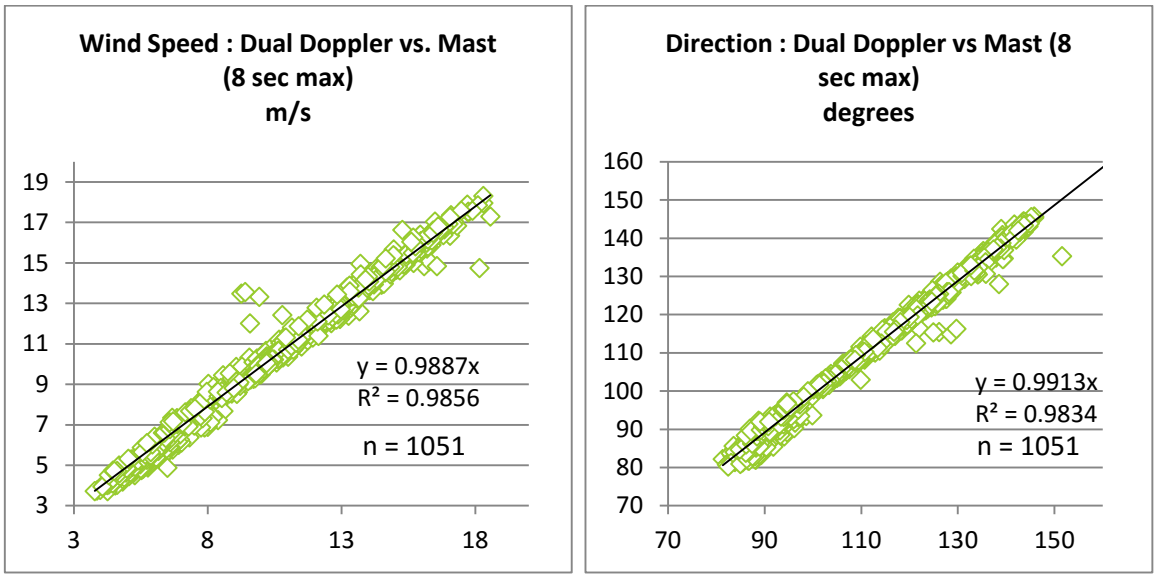

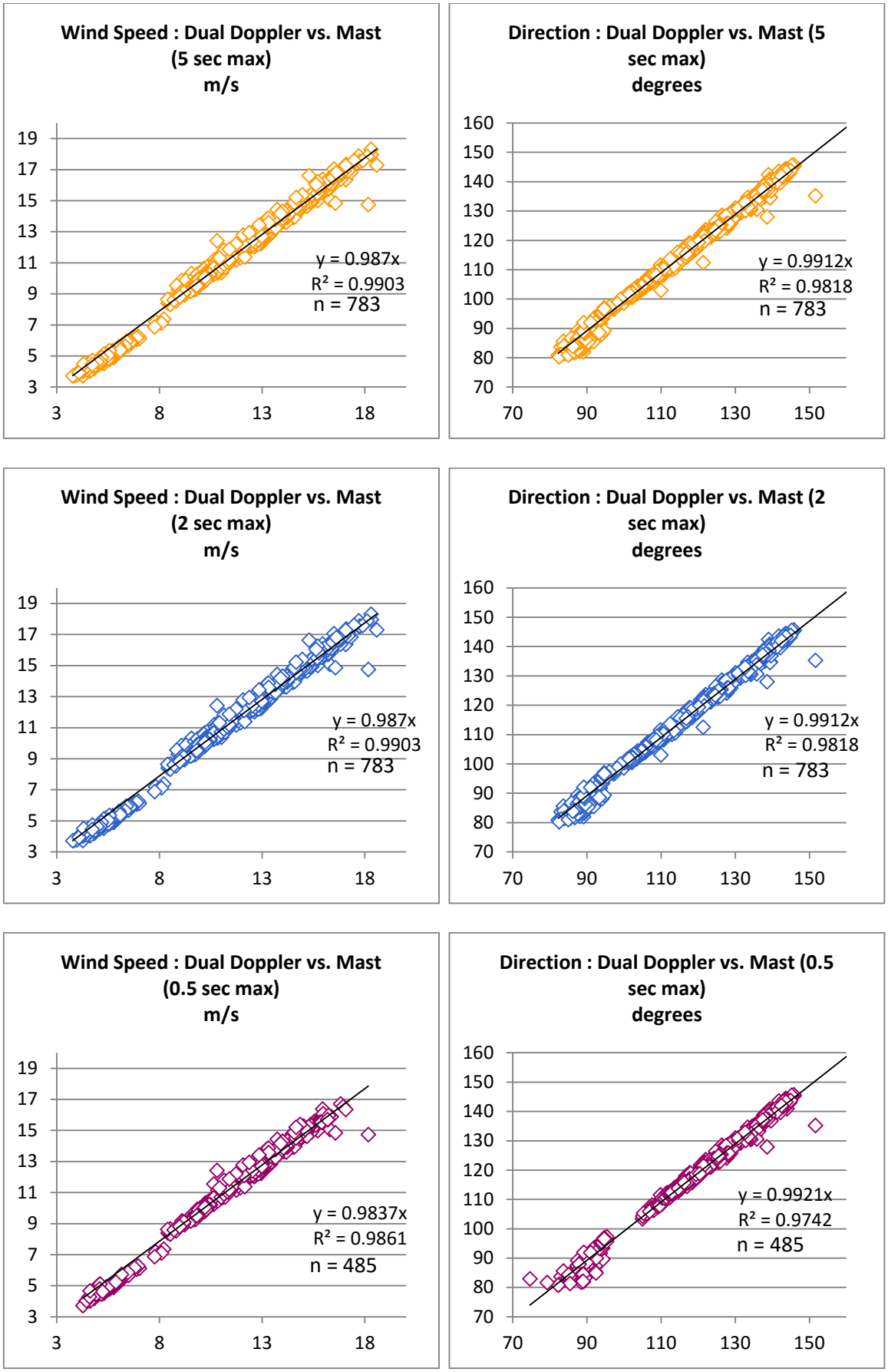

Figure 51: Simulated dual Doppler PPI results : wind speed and direction vs. cup anemometer for various time gaps